CRUSTAL AND SUB-CONTINENTAL LITHOSPHERIC MANTLE DECOUPLING BENEATH THE MALAWI RIFT

By

EMMANUEL ATEM NJINJU

Bachelor of Science in Geology

University of Buea

Buea, Cameroon

2012

Submitted to the Faculty of the
Graduate College of the
Oklahoma State University
in partial fulfillment of
the requirements for
the Degree of
MASTER OF SCIENCE
May, 2016

CRUSTAL AND SUB-CONTINENTAL

LITHOSPHERIC MANTLE DECOUPLING BENEATH

THE MALAWI RIFT

Thesis Approved:

Dr. Estella A. Atekwana

Thesis Adviser

Dr. Mohamed G. Abdelsalam

Dr. Daniel A. Laó-Dávila

ACKNOWLEDGEMENTS

I would like to express my sincere gratitude to my advisor Dr. Estella A. Atekwana for her supervision, encouragement and coaching. Without her help, this work would not have been possible. Many thanks are due to my committee members, Dr. Mohamed G. Abdelsalam and Dr. Daniel A. Laó-Dávila for their recommendations in improving my thesis. Special thanks go to Dr. Eliot A. Atekwana for his major inputs and contributions to my project.

This project is funded by the National Science Foundation – Continental Dynamics grant # EAR 1255233 "Integrated Studies of Continental Rifting: From Nascent Extension (Okavango Rift Zone) to Continental Breakup (Afar Depression)". I would like to thank Oklahoma State University and the Boone Pickens School of Geology for the excellent quality of education they offered me. I am also grateful for the scholarships awarded to me. These include the RE and KR McPhail Geology Scholarship.

Luel Emishaw, Kitso Matende, Andrew Katumwehe, and Tadesse Alemu, helped me tremendously during this study. Thanks also go to Dr. Kennedy Fozoa in the University of Buea, for acting as my source of inspiration. Dr. Pride Abongwa and Mr. Celestine Foteh made sure I was always comfortable during my stay in Stillwater.

I would like to forward my special thanks to my family, especially my wife (Elizabeth Fomenky), kids (Drake Njinju-Atem and Estella Njinju-Atem), mother (Florence Atem), brothers (Ernest Amin Atem, and Fidelis Morfaw Atem), sisters (Brunhilda Awung, Francisca Atem, Jacqueline Awah, and Delphine Funue) and to my family-in-law, especially Hygenus Fomenky and Mirabel Fomenky for their endless supply of encouragement and support throughout this project. Special thanks also go to my friends who have been a constant source of encouragement, among them, Ernest Funue, Joseph Njong and Roland Fon.

Acknowledgements reflect the views of the author and are not endorsed by committee members or Oklahoma State University.

Name: EMMANUEL ATEM NJINJU

Date of Degree: MAY, 2016

Title of Study: CRUSTAL AND SUB-CONTINENTAL LITHOSPHERIC MANTLE DECOUPLING BENEATH THE MALAWI RIFT

Major Field: GEOLOGY

Abstract:

We analyzed satellite gravity and aeromagnetic data using the two-dimensional (2D) power-density spectrum technique to investigate the lithospheric and thermal structure beneath the magma-starved Malawi Rift, which forms the southern extension of the Western Branch of the East African Rift System. We observed: (1) lack of consistent pattern of crustal thinning and elevated heat flow along the surface expression of the rift. Beneath the Rungwe Volcanic Province (RVP) in the north, the crustal thickness ranges between 40 and 45 km and varies between 35 and 40 km along the entire length of the rift. (2) shallow lithosphere-asthenosphere boundary (LAB) elevated to ~64 km beneath the entire length of the rift and deeper than 100 km beneath the surrounding Precambrian terranes reaching in places ~124 km. (3) localized zones of high heat flow (70-75 mWm^{-2}) beneath the RVP, and the central and southern parts of the rift. The central and southern thermal anomalies are due to the presence of uranium deposits in the Karoo sedimentary rocks. We interpret the crustal thickness heterogeneity to have been inherited from pre-existing lithospheric stretching, while strain during the extension of the Malawi Rift is preferentially localized in the sub-continental lithospheric mantle (SCLM). Our interpretation is supported by 2D forward modeling of the gravity data showing uniform stretching of the SCLM by a factor of 1.5 to 1.8 beneath the entire length of the rift. Our results indicate decoupling of the crust from the SCLM during the early stages of the development of the Malawi Rift.

TABLE OF CONTENTS

LIST OF TABLES

Table Page

LIST OF FIGURES

Figure Page

CHAPTER I

INTRODUCTION

Continental rifts are elongate tectonically-induced depressions within the Earth's surface underlain by a lithosphere that has been modified by extension [*Olsen,* 1995; *Thybo and Nielson,* 2009]. Hence, continental rifts are characterized by three features: surface manifestation in the form of elongated grabens, and crustal and sub-continental lithospheric mantle (SCLM) thinning [*Thybo and Nielson,* 2009]. Numerical models for continental rift initiation highlight the importance of an actively upwelling asthenosphere followed by extensive magmatic diking that soften the lithosphere and enhances lithospheric stretching [e.g., *Buck,* 2006; *Schmeling,* 2010]. These magma-assisted rifting models are supported by the occurrence of surface magmatism throughout the Northern and Eastern Branches of the East African Rift System (EARS) especially in the Afar Depression and the Main Ethiopian Rift (Figure 1) [*Ebinger and Casey,* 2001; *Casey et al.,* 2006; *Wright et al.,* 2006; *Ebinger et al.,* 2010]. However, the role of magma in the initiation of rifting within the magma-starved Western Branch of the EARS (Figure 1) has not been fully validated. There is therefore the need to consider an alternative mechanism for the origin of strain localization that can explain the formation of magma-poor rift segments.

Geological and geophysical observations from the EARS suggest that pre-existing structures play an important role in strain localization during the evolution of continental rift systems at both regional and local scales. For example in the Western Branch, studies by *Katumwehe et al.* [2015]

highlight the important role that Precambrian structures have played in the localization, segmentation and termination of the Albertine-Rhino grabens in Uganda. Strain localization in these grabens is facilitated by NE-trending Precambrian structures, while the presence of the NW-trending Precambrian Aswa Shear Zone results in the termination of the grabens further northeast. Similarly, *Leseane et al.* [2015] provide evidence suggesting that the nascent Okavango Rift Zone is developing at the boundary between two Precambrian orogenic belts (the Damaran and Ghanzi-Chobe). However, the Malawi Rift located at the southern limit of the Western Branch of the EARS (Figure 1) traverses a complex array of Precambrian orogenic belts and Paleozoic-Mesozoic Karoo structures. This has also raised the question of the role of pre-existing Precambrian structure in strain localization. Thus the origin of strain localization of the magma-starved Western Branch of the EARS remains enigmatic due to the paucity of geophysical observations of the deep crust and SCLM underlying these structures. Resolving the causes and mechanics of rift initiation within magma-starved rift segments requires investigation of the lithospheric and thermal structure beneath the rift, including imaging of sharp interfaces such as the Moho and the lithosphere-asthenosphere boundary (LAB).

This study aims at investigating the lithospheric and thermal structure beneath the Malawi Rift and surroundings in order to provide constrains that will better the understanding of the mechanism of strain localization at the early stages of the evolution of magma-starved rift segments. The Malawi Rift, which represents the southern part of the Western Branch of the EARS (Figure 1), is an ideal place for such study because: (1) it is the youngest segment of the Western Branch of the EARS, and it is magma-starved with the only magmatism limited to the Rungwe Volcanic Province (RVP) at its northern tip. (2) The rift is developing within Precambrian and Paleozoic-Mesozoic structures with different orientations allowing for the examination of the possible influence of pre-existing structures on the current structure and thermal status of the crust and the SCLM. (3) Previous studies suggest that the rift is propagating

from north to south with maximum extension rates in the north [*Calais et al.*, 2006, *Stamps et al.*, 2008; *Saria et al.*, 2014]. This allows for the evaluation of the along strike variability in the lithospheric structure beneath the rift, and how this controls rift evolution.

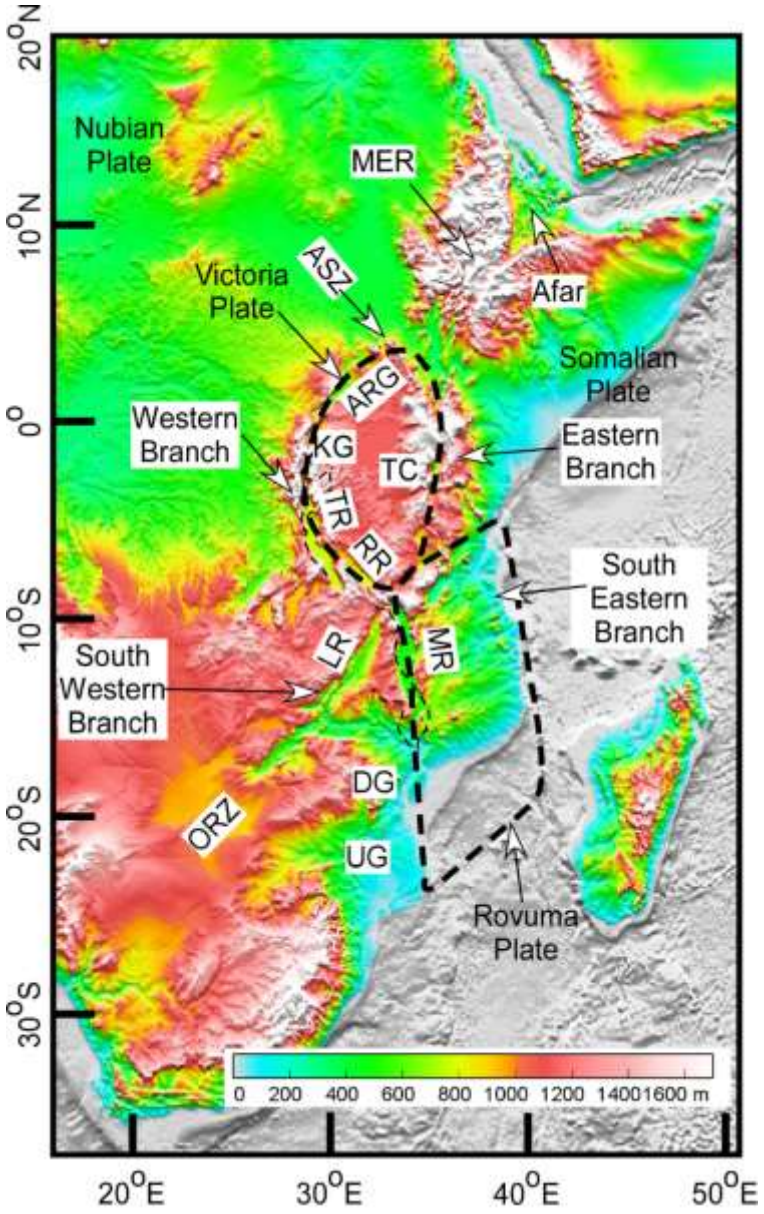

Figure 1: Digital Elevation Model (DEM) extracted from the Global 30 Arc Second Elevation Data (GTOPO30) showing the East African Rift System (EARS) and the Eastern and Western branches of the EARS. MER = Main Ethiopian Rift. ASZ = Aswa Shear Zone. ARG =

Albertine-Rhino Graben. KG = Kivu Rift. TR = Tanganyika Rift. TC = Tanzanian Craton. RR = Rukwa Rift. MR = Malawi Rift. LR = Luangwa Rift. DG = Dombe Graben. UG = Urema Graben. ORZ = Okavango Rift Zone. Modified after *Leseane et al.* [2015].

This work uses the two-dimensional (2D) power-density spectrum analysis of satellite gravity and aeromagnetic data to determine the lithospheric and thermal structures, respectively beneath the Malawi Rift and surroundings. This study then constructs 2D forward model of the satellite gravity data in order to reconcile the observed lithospheric structure. This work presents for the first time detailed imaging of the lithospheric and thermal structure of the Malawi Rift and surroundings which suggests that the crustal structure is inherited from pre-existing lithospheric stretching, while extensional strain is preferentially and uniformly localized within the SCLM by a factor of 1.5 to 1.8 during the Neogene Malawi rift related extension. This suggest for the first time extensional decoupling of the crust from the SCLM during the evolution of the Malawi Rift.

CHAPTER II

TECTONIC SETTING

The Neogene Malawi Rift forms the southern terminus of the Western Branch of the EARS (Figure 1). The EARS constitutes a system of narrow rifts that represents the full spectrum of continental rifting from the initial stages of continental rifting in Okavango in Botswana to incipient seafloor spreading in the Afar in Ethiopia. The EARS begins in Afar, characterized by an ~E-W extension of the Somalian Plate relative to the Nubian Plate at a rate of ~5-6 mm/yr with a general southward decrease in extension [e.g., *Stamps et al., 2008; Saria et al.,* 2014]. From Afar, the EARS trends southward as the Main Ethiopian Rift where it bifurcates further south into the Eastern and Western Branches. It is suggested that the Western Branch was initiated ~12 Ma ago, later than the ~20 Ma rift initiation of the Eastern Branch [*Ebinger,* 1989*; Cohen et al.,* 1993]. However, recent study suggests that the initiation of both branches was coeval at 25 Ma [e.g., *Roberts et al.,* 2012].

Unlike the Eastern Branch, the Western Branch is characterized by deeper and larger magnitude earthquakes [*Craig et al.,* 2011]. It extends southward for ~ 3000 km from the NNE-trending Albertine and Rhino grabens through the N-trending Kivu graben into the NW-trending Tanganyika Rift (Figure 1). It continues south-eastward as the NW-trending Rukwa Rift following the NW-trending tectonic fabric of the Paleoproterozoic Ubendian Belt before merging into the dominantly N-S trending Malawi Rift (Figure 2).

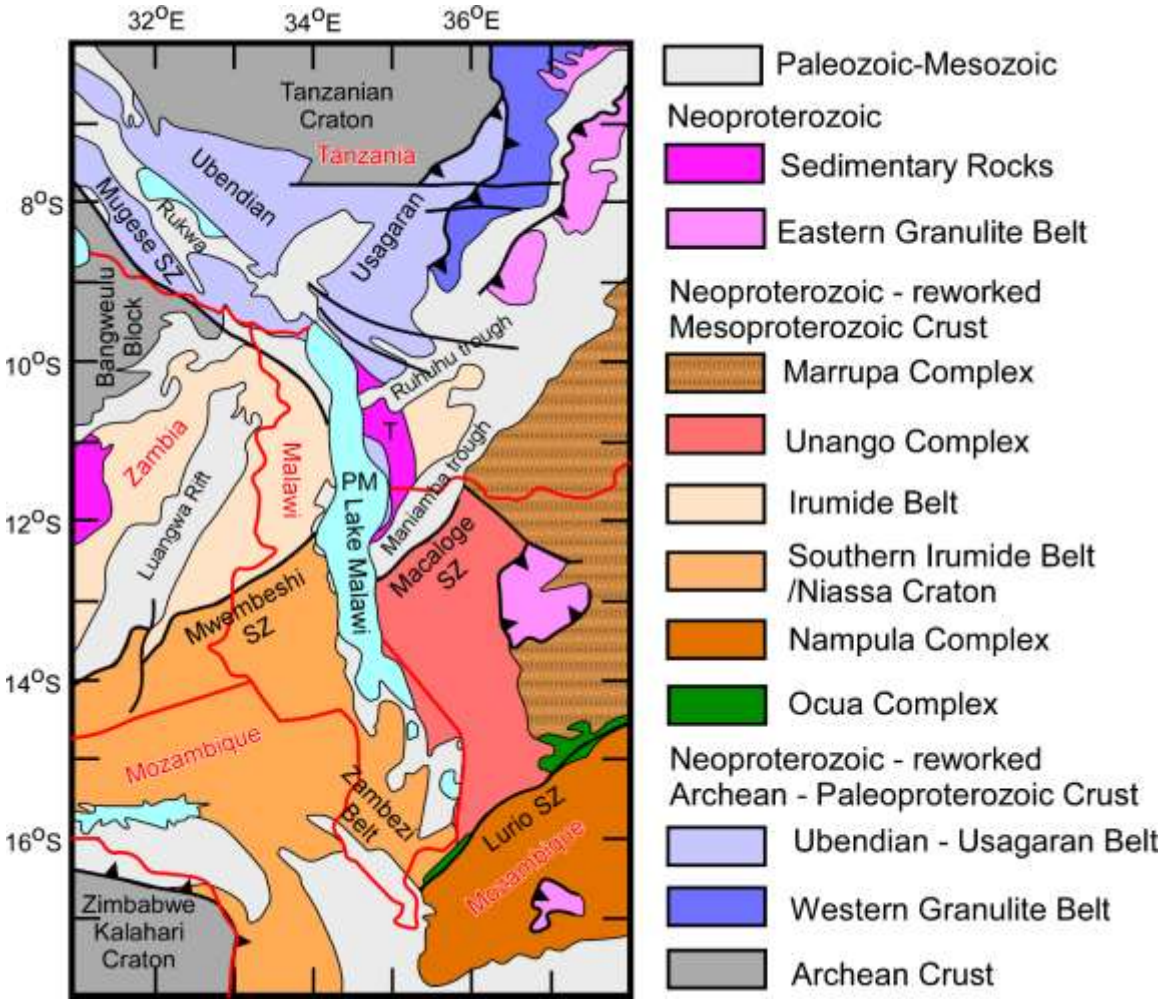

Figure 2. Tectonic map showing the exposures of the Precambrian and Paleozoic-Mesozoic units around the Malawi Rift. Modified after *Fritz et al.* [2013] and *Laó –Dávila et al.,* [2015]. T = Txitonga Group. PM = Ponta Messuli Complex.

2.1. The Malawi Rift

The Malawi Rift extends for over 900 km from the RVP in the north to the Dombe and Urema grabens in the south [*Ebinger et al.,* 1987; *Ring et al.,* 1992*; Chorowicz,* 2005]. It is largely amagmatic and the Pliocene-Pleistocene RVP represents the only volcanic center associated with the rift [*Ebinger et al.,* 1989]. The first 550 km stretch of the rift is occupied by Lake Malawi

with width ranges between 50 and 75 km. In the north, the rift strikes NNW and then continues with a general N-S trend before assuming a NNE-trend at its southern end (Figure 3).

Based on its geometry, *Ebinger et al.* [1987] divided the Malawi Rift into five broad segments. Differently, a recent study by *Laó–Dávila et al.* [2015] suggests eight segments bounded by curvilinear border faults (Figure 3). The most pronounced border fault system is the ~120 km long Livingstone Fault located at the northern tip of the eastern side of the rift (Figure 3). Tilting of the Livingston Fault caused fracturing of the hanging wall producing the 2009 Karonga earthquake that caused severe damage to the infrastructure of the Karonga region [*Biggs et al.*, 2010; *Fagereng*, 2013]. The Karonga Fault in the western flank of the northern segment of the rift extends for 17.8 km to the SE (Figure 3) [*Biggs et al.*, 2010]. The western side of the center of the rift is bounded by the ~200 km-long Usisya Fault (Figure 3) [*Contreras et al.*, 2000; *Laó–Dávila et al.*, 2015]. The Bilila-Mtakataka Fault located at the southwestern end of the rift is ~125 km long (Figure 3) [*Jackson and Blenkinsop*, 1997]. Deep earthquakes (>30 km) have been recorded in Malawi, due to the rupture of the Bilila-Mtakataka fault in a single seismic event [*Jackson and Blenkinsop*, 1997].The Mwanza Fault located at the southern end of the rift (Figure 3) is interpreted as a NW-striking transcurrent fault [*Castaing*, 1991].

It is suggested from surface geological studies that rivers originally flowing eastward and northeastward across Malawi were captured by the rift [*Chorowicz and Sorlien*, 1992]. These rivers infilled the rift with fluviatile deposits eroded from the Precambrian terranes and the Karoo sedimentary rocks [*Flannery and Rosendahl*, 1990; *Betzler and Ring*, 1994]. The most prominent Karoo sedimentary basins around the Malawi Rift are the Luangwa Rift, the Ruhuhu and Maniamba troughs, the Shire Graben and the Zambezi Rift (Figure 3). Seismic data suggests that in the northern part of the rift adjacent to the Livingstone Fault (Figure 3), sediment thickness can reach up to 4.5 km and becomes thinner southward [*Specht and Rosendahl*, 1989; *Flannery and Rosendahl*, 1990].

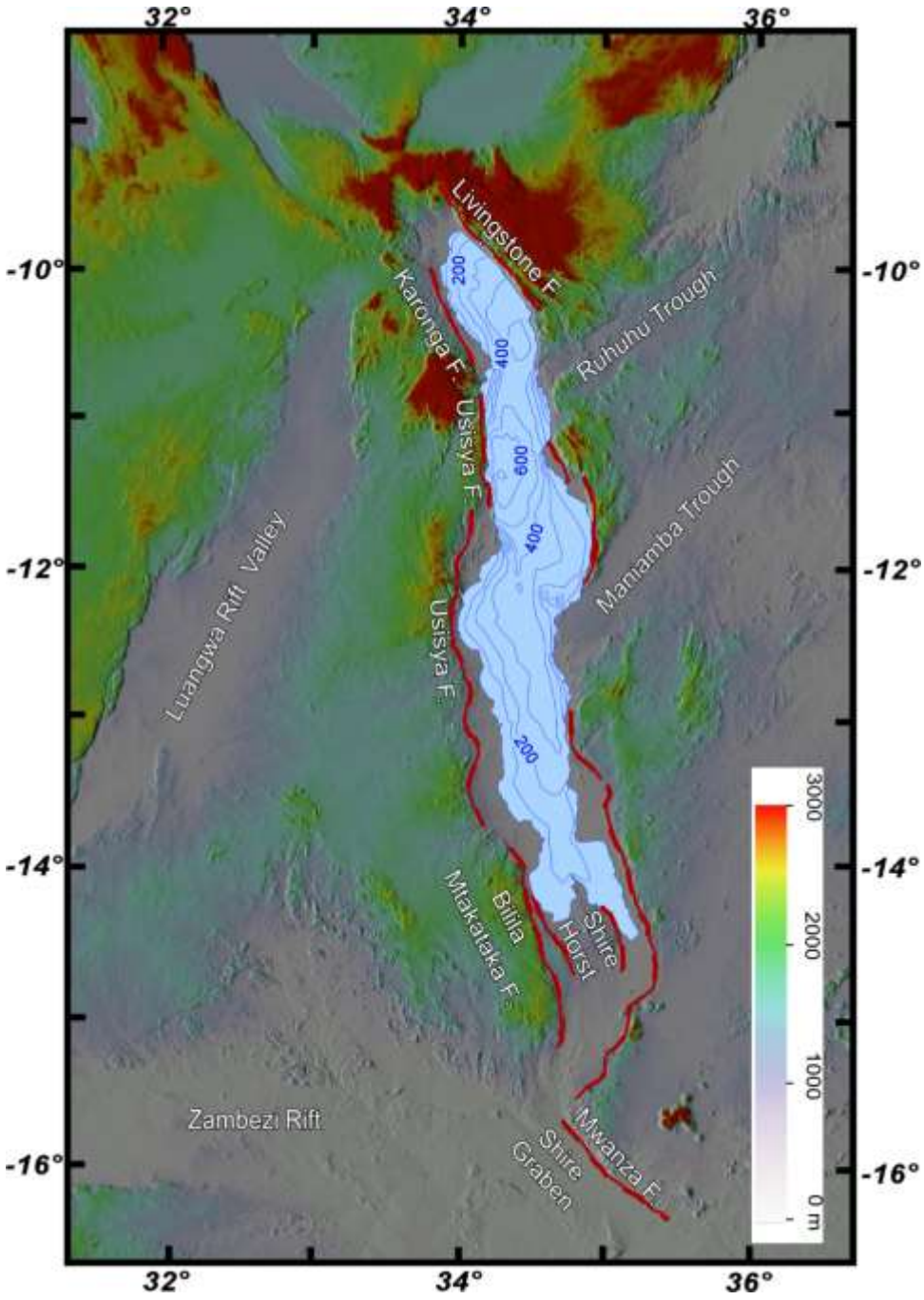

Figure 3. Shuttle Radar Topography Mission (SRTM)-Digital Elevation Model (DEM) of the Malawi Rift showing the border faults and the surrounding Paleozoic-Mesozoic Karoo rift basins. Blue contour lines show water depth within Lake Malawi. F = Fault.

Based on radiometric dating using $^{40}Ar/^{39}Ar$ systematics of samples from the RVP, *Ebinger et al.* [1993] concluded that rifting at the northern tip of the Malawi Rift started ~8.6 Ma, with volcanism continuing to the present. However, recent dating of the RVP by *Mesko et al*. [2014] suggests that rifting at the northern tip of the Malawi Rift started ~18 Ma, much earlier than previously suggested. Previous studies have observed a southward decrease in the amount of basin's subsidence, thickness of the Cenozoic-Quaternary sedimentary rocks, and elevation of the topographic escarpments. These are considered to indicate that the northern part of the Malawi Rift is older than its southern part and provide evidence for southward propagation of the rift and its opening in a "zipper-like" fashion from north to south [*Flannery and Rosendahl*, 1990; *Ring and Betzler*, 1995]. This is supported by recent geodetic studies which suggest that the rift is extending at a surface velocity of 2.2 mm/year in the north and 1.5 mm/year in the south due to an eastward movement of the Rovuma Plate away from the Nubian Plate (Figure 1) [*Saria et al.*, 2014].

The Malawi Rift traverses a complex array of Precambrian orogenic belts and Paleozoic-Mesozoic Karoo sedimentary basins (Figure 2). *Laó–Dávila et al.* [2015] developed a segmentation model which suggests that lithospheric heterogeneity has led to a hierarchical segmentation of the Malawi Rift. In its northern section, the Malawi Rift strikes NNW, paralleling the tectonic fabrics of the Paleoproterozoic Ubendian Belt [*Ring*, 2002; *Laó–Dávila et al.*, 2015]. The NNW-trending Mugese Shear Zone which consist mainly of metadioritic gneiss with steeply dipping foliations [*Ring*, 2002] separates the Ubendian Belt from the NE-trending Mesoproterozoic Irumide Belt (Figure 2) [*Fritz et al.*, 2013]. The Paleoproterozoic Ponta Messuli Complex that is exposed on the eastern side of the rift (Figure 2) is suggested to be the southernmost extension of the Ubendian Belt [*Fritz et al.*, 2013; *Laó–Dávila et al.*, 2015].

Unlike the northern section of the Malawi Rift, the rift is at high angle to the tectonic fabrics of the Precambrian entities located to the south of the Mwembeshi Shear Zone and the Macaloge

Shear Zone (Figure 2) [*Laó–Dávila et al.,* 2015]. The Mwembeshi Shear Zone represents the boundary between the Irumide Belt in the NW and the Southern Irumide Belt to the SE (Figure 2) [*Fritz et al.*, 2013]. Both belts are Mesoproterozoic in age with the only difference being the absence of mid-Mesoproterozoic plutonic rocks within the Southern Irumide Belt [*Fritz et al.*, 2013; *Laó–Dávila et al.,* 2015]. However, a pre-Mesoproterozoic cratonic block (the Niassa Craton) is suggested to be located southeast of the Mwembeshi Shear Zone [*Andreoli*, 1984; *Daly*, 1986; *De Waele et al.*, 2006].

The Macaloge Shear Zone exposed to the southwestern edge of the Karoo Maniamba Trough separates the continuation of the Irumide Belt in southern Tanzania from the Neoproterozoic Pan-African Mozambique Orogenic Belt in Mozambique. Along the eastern margin of the Malawi Rift, the regional structural grains of the Mozambique Orogenic Belt regionally parallels the rift axis [*Daly*, 1986]. The Mozambique Orogenic Belt, which is sandwiched between fragments of East and West Gondwana [*Meert*, 2003] have been divided into the Unango, Marrupa, and Nampula complexes which contain a variety of orthogneisses which are over-thrust by the Eastern Granulite Belt (Figure 2) [*Bingen et al.*, 2009].

Further south of the Southern Irumide Belt close to the Zimbabwe-Kalahari Craton (Figure 2) the structural trend of the Precambrian structures changes from northeast to northwest. This NW-trending structure constitute the Neoproterozoic Pan-African Zambezi Belt [*Hanson et al.*, 1994; *Hargrove et al.*, 2003]. The Zambezi Belt is thought to be the westward continuation of the Lurio Belt [*Sacchi et al.,* 2000]. However, the relationship between the Lurio and Zambezi Belts is obscured by Karoo rifts (Shire Graben and Zambezi Rift), and the Cenozoic Malawi Rift [*Sacchi et al.,* 2000]. The NW-trending Karoo Shire Graben is suggested to have stopped the Malawi Rift from propagating further south [*Chorowicz and Sorlien* 1992].

CHAPTER III

DATA AND METHODS

3.1. Depth to Moho and lithosphere-asthenosphere boundary analyses

Magnetotelluric (MT) and seismic techniques have been traditionally used to estimate the Moho and LAB depth [e.g., *Wölbern et al.,* 2012; *Jakovlev et al.,* 2013; *Mulibo and Nyblade,* 2013]. Due to the expense and time needed for data collection these techniques mostly investigate the lithospheric structure along profiles limiting their application for investigating large areas. Using power density spectral analysis of satellite gravity data to determine the crustal thickness (depth to the Moho) and depth to LAB offers an affordable and reliable alternative [e.g., *Gómez-Ortiz et al.,* 2011]. In addition, the recent availability of global coverage of satellite gravity data allows the determination of the lithospheric structure over wide areas.

This study used satellite gravity data extracted from the World Gravity Map 2012 (WGM2012) [*Balmino et al.,* 2012; *Bonvalot et al.,* 2012] to estimate the depth to Moho and the LAB beneath the Malawi Rift and surroundings. The WGM2012 model has a spatial resolution of ~9 km. To take into account the real topography of the Earth which is approximated to a spherical prism, the global Bouguer gravity data was computed using the spherical terrain correction instead of the regular slab correction [*Balmino et al.,* 2012]. This involves subtracting the Earth's TOPography derived gravity model (ETOPG1) from the Earth Gravity Model 2008 (EGM2008). The EGM2008 comprises surface gravity measurements (land, airborne, and marine surveys), and

measurements from satellite altimetry and satellite gravimetry (GRACE mission) [*Bonvalot et al.,* 2012]. ETOPG1 is obtained from the spherical harmonic analysis of the heights of the Earth's topography-bathymetry components from the 1°X1° spatial resolution Global Topographic 30 arc second (GTOPO30) database. GTOPO30 is the global digital elevation data sets. The Bouguer gravity data is gridded using the minimum curvature method [*Briggs,* 1974] to produce a Bouguer gravity anomaly map (Figure 4).

The observed Bouguer gravity anomaly is the sum of gravity anomalies due to lateral variations in density within different lithological units in the near-surface and deeper within the Earth. It is, therefore essential to identify contributions due to lateral variations in density occurring at different depths [*Gómez-Ortiz et al.,* 2011]. High-frequency components of the observed gravity anomalies are attributed to shallow depths, and low-frequency components are attributed to deep depths. This is because the deeper the gravity source, the weaker the signal (low frequency) as the energy due to the force of attraction between the gravity source and the sensor is spread over a wider spectrum.

The observed Bouguer gravity data was upward continued to 2 km in order to attenuate the unwanted high-frequency anomalies due to near-surface (<1 km) features, while accentuating deep-source low-frequency anomalies. This work used the 2D radially averaged power spectrum analysis developed by *Tselentis et al.,* [1988] for the estimation of the depth to Moho and the LAB beneath the Malawi Rift and surroundings. The Power spectrum of gravity describes how the power of the gravity response is distributed over different frequencies (or wavenumbers) [*Russo and Speed,* 1994]. In this study the 2D radially averaged power spectrum of the upward continued gravity data is calculated for 1^{o} x 1^{o} (110 X 110 km) overlapping windows. Prior to calculating the power spectrum, the gravity data for each window was transformed from the space domain to the frequency domain by means of a Fast Fourier Transform (FFT). This transformation engenders the Gibbs phenomena in which the boundaries of the windows behave

as a jump discontinuity (edge effect). The windows were overlapped by 50 % on all sides in order to minimize the Gibbs phenomena. The Malawi Rift has a maximum width of 75 km, which fits in a 1^{o} x 1^{o} window. Using a larger window size would result in biases from noise or unwanted regions and would also average structures that may be heterogeneous.

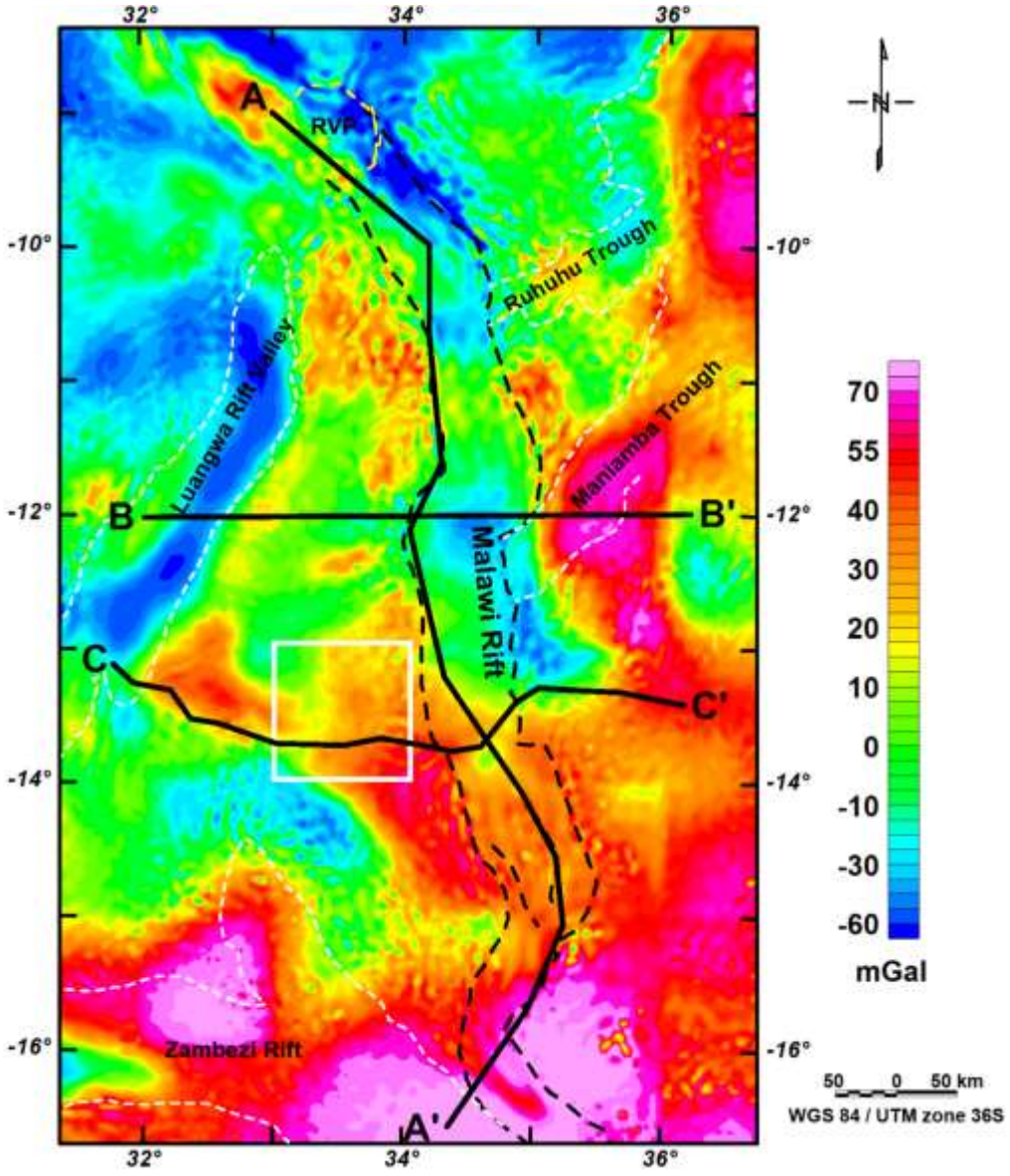

Figure 4. Satellite Bouguer gravity anomaly map extracted from the World Gravity Map 2012 (WGM 2012) used for estimating the depth to Moho, and the lithosphere-asthenosphere boundary (LAB) beneath the Malawi Rift and surroundings using two-dimensional (2D) radially averaged

power spectrum analysis. White box represents the location of the 1^0 x 1^0 block used for the generation of the power spectrum curve in Figure 4. The black dash lines represent the outline of the Malawi Rift as appears on the Shuttle Radar Topography Mission (SRTM)-Digital Elevation Model (DEM) in Figure 3. The black lines A-A', B-B' and C-C' show the trace of the lithospheric–scale 2D forward gravity models presented in Figures 13 to 15. Dotted white lines represent the outline of Paleozoic-Mesozoic (Karoo-aged) rift structures. Dotted yellow outline represents the Rungwe Volcanic Province (RVP).

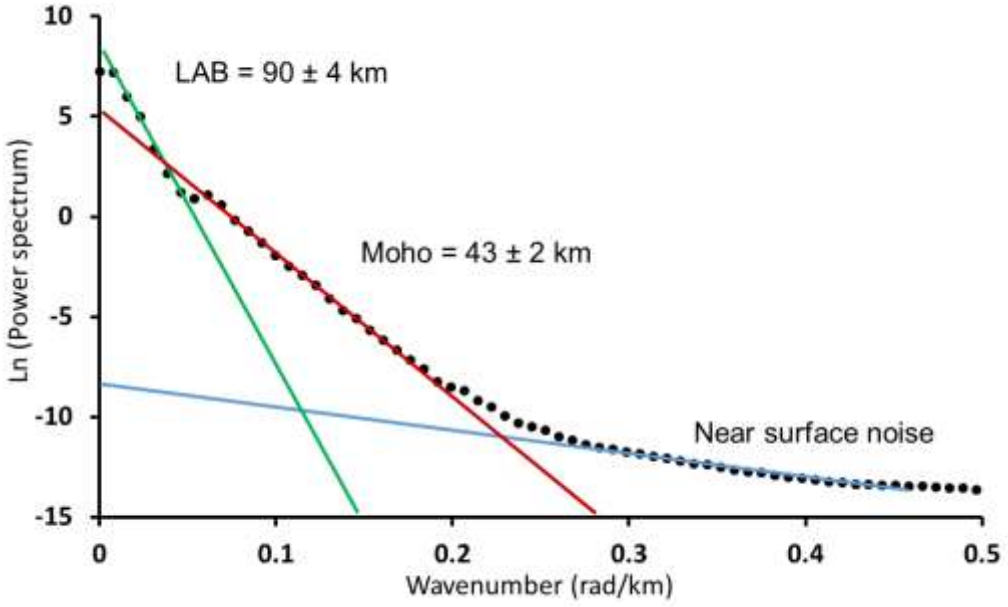

Figure 5. An example of the two-dimensional (2D) radially averaged power spectrum analysis curve used for the estimation of the depth to Moho and the lithosphere-asthenosphere boundary (LAB). The curve is a plot of the logarithm of the radially averaged power spectrum against wavenumber. The curve shows three linear segments. The intermediate segment is used to calculate the crustal thickness (depth to Moho). While the steepest segment is used to calculate the Lithopshere-Asthenosphere Boundary (LAB). See Figure 4 for location.

The solution spectral curve for each window is generated by plotting ln(power spectrum) against the wavenumber (*k*) (Figure 5). The spectral curves are characterized by three linear segments

and breaks in their slopes representing density discontinuities at different depth levels [*Fairhead and Okereke,* 1987*; Tselentis et al.,* 1988*; Gómez-Ortiz et al.,* 2005*;* 2011]. Each of the linear segments is associated with a range of wavenumber and provides an indication of their average depth [*Gómez-Ortiz et al.,* 2005*;* 2011]. The lowest wavenumber segment represents a sharp density contrast between the lithosphere and the asthenosphere, while the intermediate wavenumber portion corresponds to the sharp density contrast between the crust and the mantle, and the highest wavenumber segment corresponds to shallow causative bodies or noise contained in the data. This work determined the depth to the crust-mantle discontinuity (Moho) from the slope of the intermediate linear segment [*Tselentis et al.,* 1988; *Sanchez-Rojas and Palma,* 2014], and the depth to the LAB from the slope of the steepest segment [*Gómez-Ortiz et al.,* 2005*;* 2011].

To avoid uncertainties associated with selecting the part of the intermediate linear segment where the slope is calculated, three first-order polynomial fits were used to produce straight lines in the intermediate segment, and the average slope of these lines was taken to represent the depth to Moho. Similarly in the steepest linear segment of the spectral curve, three first-order polynomial fits were used to produce straight lines, and the average slope of these lines was taken to represent the depth to the LAB. Subsequently, for the corresponding linear segment, the standard deviation of each fit was determined. The combination of the variations of the slope measurements from the three different polynomial fits and their standard deviations led to the determination of the error in estimating the depth to Moho and LAB at ~ ± 2 km and ~ ± 4 km, respectively.

In order to test the reliability of the estimates of the depth to Moho and the LAB obtained from the 2D radially averaged power spectrum of WGM2012 satellite gravity data using 50% overlapping windows, the data were reanalyzed using 90% overlapping windows. The results for the 90% overlapping windows agree within 1 to 3 km with those estimated from the 50% overlapping windows. Given that there is no published crustal thickness of the Malawi Rift, the

validity of the 2D radially averaged power spectrum technique in Moho depth determination is tested in the Okavango Rift Zone where there are published seismic constraints. For this, the WGM2012 satellite gravity data for the Okavango Rift Zone were obtained and used in calculating the crustal thickness

Table 1. Crustal thickness in the Okavango Rift Zone estimated from two-dimensional (2D) radially averaged power spectrum analysis of the satellite gravity data compared with the crustal thickness estimates from passive seismic study [*Yu et al.*, 2015].

Station	Latitude (deg)	Longitude (deg)	[*Yu et al.,* 2015] (km)	Gravity method (km)
B12SS	-18.746	22.197	46.2 ± 0.5	44.5 ± 2
B13NX	-18.579	21.994	46.6 ± 0.4	43.9 ± 2
B14MH	-18.295	21.792	45.8 ± 0.3	45.9 ± 2
B06OR[a]	-19.901	23.527	43.6 ± 0.5	46.9 ± 2
B07DX[b]	-20.549	22.649	40.5 ± 0.5	41.1 ± 2
B08TS[c]	-20.164	22.459	37.8 ± 1.0	38.8 ± 2
B09NK	-19.663	22.194	41.8 ± 0.2	37.9 ± 2
B10PP	-18.913	22.543	39.9 ± 0.5	38.5 ± 2
B11ET[b]	-19.016	22.316	44.3 ± 0.5	45.7 ± 2
B15MW[c]	-19.631	23.827	34.0 ± 0.4	33.9 ± 2
B17CI[c]	-19.294	22.909	38.8 ± 0.5	37.7 ± 2
B03SL	-21.121	24.764	40.8 ± 0.3	39.9 ± 2
B04KH	-20.474	24.514	42.6 ± 0.7	43.4 ± 2
B05MO	-20.218	24.132	40.7 ± 0.2	42.6 ± 2
B01KR	-22.238	26.718	43.7 ± 0.2	42.7 ± 2
B02LT	-21.393	25.581	42.8 ± 0.3	43.3 ± 2
B1665	-22.825	27.229	42.6 ± 0.3	42.7 ± 2
SA64	-22.969	26.202	41.5 ± 0.4	42.2 ± 2
SA65	-22.818	27.222	42.7 ± 0.3	42.7 ± 2
SA66	-21.900	26.373	44.7 ± 0.4	41.3 ± 2

[a]Using RFs with back azimuth between 45 and 225^0

[b]Using RFs with back azimuth of $0–45^0$ and $225–360^0$

[c]After applying the reverberation-removal technique.

of twenty 1° x 1° windows centered on the locations of passive seismic stations for which the crustal thickness had been determined from joined receiver function analysis and gravity modeling [*Yu et al.*, 2015]. A comparison of the results of the two approaches (Table 1 and Figure 6) indicates that the Moho depth estimates from the 2D radially averaged power spectrum method is in good agreement with those obtained from the passive seismic data with root-mean-square (RMS) error of ~2 km.

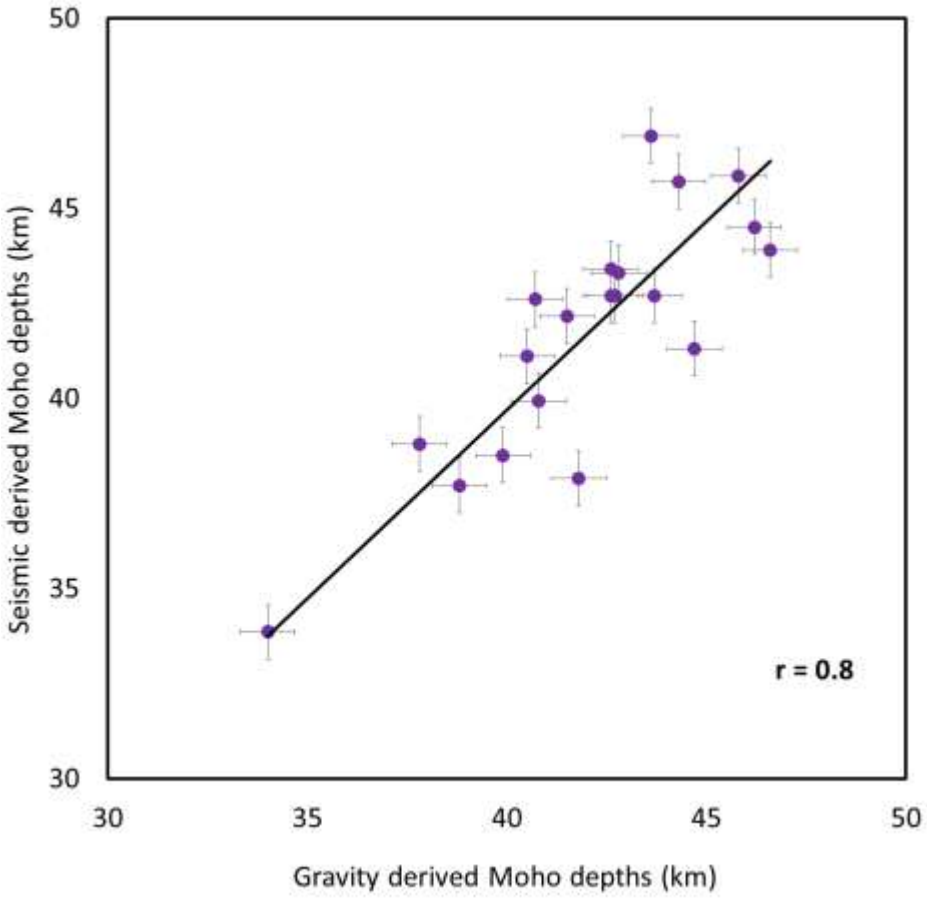

Figure 6. A cross plot showing the comparison between depths to Moho estimated from the two-dimensional (2D) radially averaged power spectrum analysis of the satellite gravity data in the Okavango Rift Zone, with depths to Moho determined from seismic receiver functions study [*Yu*

et al., 2015]. Horizontal and vertical bars crossing the graph points represent the error margins in the estimates of the two methods.

Gómez-Ortiz et al., [2011], had shown that the LAB depth beneath the Iberian Peninsula estimated from the 2D radially averaged power spectrum method are in good agreement with those determined from S-wave tomography and P-wave velocity data obtained by different studies such as those of *Fullea et al.* [2010].

3.2. Curie Point Depth Analysis

The Curie point depth (CPD) is the depth at which materials within the crust and upper mantle reach their Curie Point or temperature at which magnetic minerals lose their ferromagnetization to become paramagnetic, and it is usually taken to be 580 ^{0}C for magnetite [*Ross et al.,* 2006]. The CPD is related to either heat flow or geothermal gradient, or to the thermal properties of the lithosphere [*Aboud et al.,* 2011*; Arnaiz-Rodriguez and Orihuela,* 2013].

This study used aeromagnetic data to estimate the Curie Point Depth (CPD) beneath the Malawi Rift and surroundings, and subsequently utilized the CPD as a proxy for the heat flow determination. The aeromagnetic data for this study is a merged grid obtained from the Council of Geoscience, South Africa and include aeromagnetic data collected by the Government of Malawi between 1984 and 1985 through E-W transects with 1 km line spacing, 10 km tie lines, and 120 m terrain clearance. No data was collected over Lake Malawi. However, over the lake, satellite total magnetic intensity data was extracted from the Geosoft server, and downward continued to 120 m (the flight altitude of the aeromagnetic data) and merged with the aeromagnetic data. The total magnetic intensity from these merged data is shown in Figure 7.

Two main techniques have been developed to estimate the CPD. These techniques include those that examine the shape of isolated magnetic anomalies [e.g., *Bhattacharyya and Lue,* 1975] and

those that examine statistical patterns of magnetic anomalies [e.g., *Spector and Grant*, 1970].

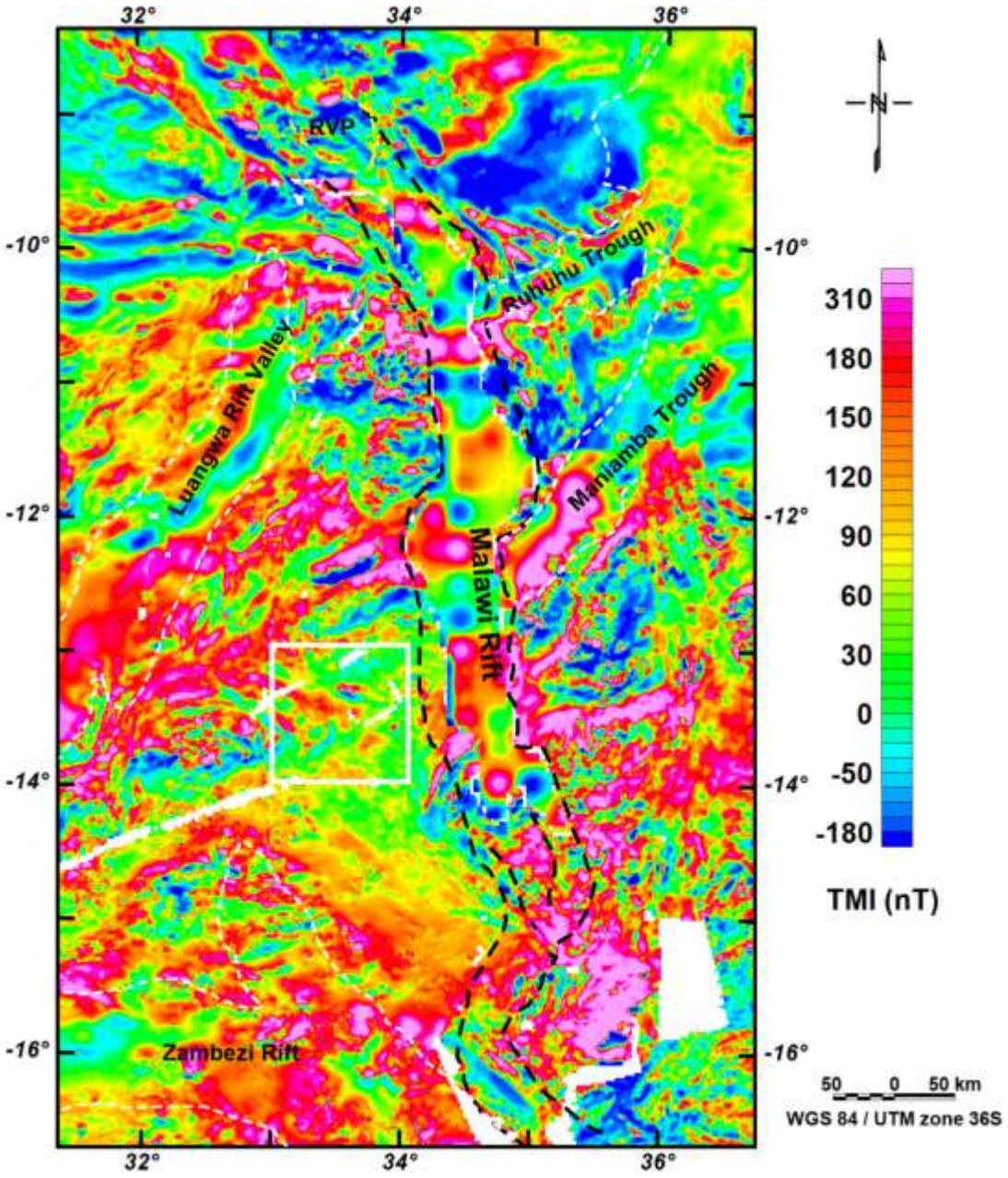

Figure 7. Map of total magnetic intensity of the aeromagnetic data used for estimating the Curie Point Depth (CPD) beneath the Malawi Rift and surroundings using two-dimensional (2D) radially averaged power spectrum analysis. White box represents the location of the 1^0 x 1^0 block used for the generation of the power spectrum curves in Figure 8. The black dash lines represent

the outline of the Malawi Rift as appears on the Shuttle Radar Topography Mission (SRTM) Digital Elevation Model (DEM).

Both methods provide the relationship between the 2D radially averaged power spectrum of magnetic anomalies and the depth of the magnetic source by transforming the spatial data into frequency domain by means of FFT. The statistical method is more appropriate for regional studies of CPD [*Shuey et al.,* 1977*; Blakely,* 1988].

This study estimated the CPD using the statistical method which relates the 2D radially average power spectrum of magnetic anomalies to the depth to the base of the magnetized sources [*Spector and Grant,* 1970; *Shey et al.,* 1977; *Okubo et al.,* 1985; *Tanaka et al.,* 1999; *Tanaka and Ishikawa,* 2005; *Manea and Manea,* 2011; *Hussein et al.,* 2013]. This work calculated the 2D radially average power spectrum of magnetic anomalies in 1^o x 1^o (~110 km x 110 km) 50% overlapping windows on all sides in order to provide more consistent results [*Tanaka et al.,* 1999], and also to reduce edge effects due to Gibbs phenomenon.

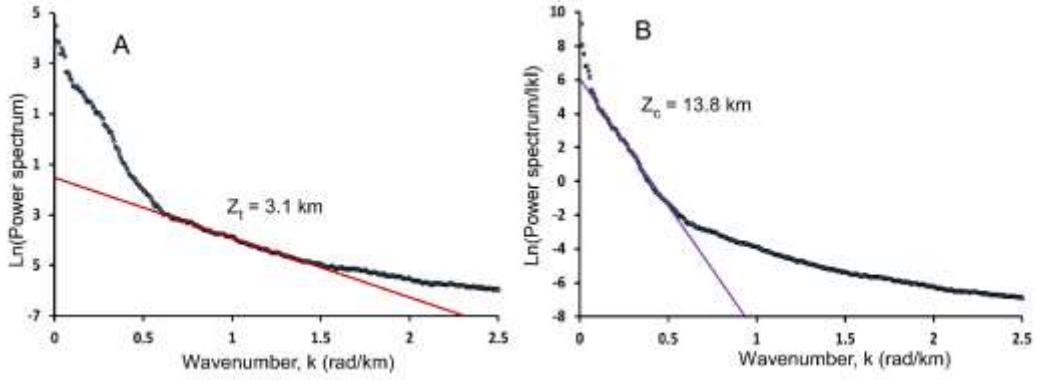

Figure 8. Example of the two-dimensional (2D) radially averaged power spectrum analysis curve (A) for the depth to the top (Z_t) of the magnetic source and (B) for the depth to the centroid (Z_c) of the magnetic source that were used to estimate the Curie Point Depth (CPD) for the 1^o x 1^o (110km x110 km) window shown in Figure 5.

Previous studies [e.g., *Okubo et al.*, 1985] showed from the calculated 2D radially averaged power spectra, that the CPD values can be estimated by: (1) Determining the depth to the top (Z_t) of the magnetized crust by plotting (ln[Power spectrum]) against the wavenumber (k) (Figure 8A) and calculating the slope of the linear fit at the higher wavenumber portions (e.g., 0.7-1.4 rad/km) of the curve; (2) Determining the depth to the centroid (Z_c) of the magnetized crust in a similar fashion by plotting (ln[power spectrum/|k|]) against k (Figure 8B) and calculating the slope at the lower wavenumber portions (e.g., 0.10-0.31 rad/km) of the curve. The CPD or depth to the base of the magnetized crust, Z_b is given by:

$$Z_b = 2Z_c - Z_t$$

To determine the accuracy of the calculated CPD values, the statistical error is calculated for each window from the standard deviation of the slopes of three linear fits used when determining the gradients for Z_t and Z_c from the spectral curves. The error ranges in this study are found to be from 0.02 to 0.15 km for Z_t, and from 1.8 to 3.1 km for Z_c.

3.3. Heat flow estimation from Curie Point Depths

The CPDs can be used as a proxy for imaging the thermal structure of the lithosphere [*Ross et al.*, 2006].

Assuming that the temperature gradient is constant between the Earth's surface and the Curie isotherm, the one-dimensional (1D) Fourier's Law of heat conduction takes the form [e.g., *Turcotte and Schubert*, 1982]:

$$q = \mathrm{k}\frac{\mathrm{dT}}{\mathrm{dz}} \qquad (1)$$

where q is heat flux in mWm^{-2}, k is thermal conductivity in $Wm^{-1}K^{-1}$, T is temperature in K, z is depth in km, and $\frac{\mathrm{dT}}{\mathrm{dz}}$ is temperature gradient in K/km.

Tanaka et al. [1999] defined the Curie temperature, *C* as:

$$C = \mathrm{D}\frac{\mathrm{dT}}{\mathrm{dz}} \qquad (2)$$

where D is the CPD value in km.

Curie temperature is the temperature at which magnetic minerals lose their ferromagnetization to become paramagnetic. The Curie temperature of magnetite, the most abundant magnetic mineral in the crust, is approximately 580ºC [*Hunt et al.*, 1995; *Ross et al.*, 2006].

Combining equation (1) and (2), generates an equation that relates heat flow to CPD given by:

$$q = \frac{kC}{\mathrm{D}} \qquad (3)$$

The heat flow is calculated at each CPD using equation (3) assuming a Curie temperature of 580 ^{0}C [e.g., *Tanaka et al.,* 1999*; Ross et al.,* 2006; *Hussein et al.,* 2013; *Leseane et al.,* 2015]. The thermal conductivity (*k*) is also a variable and depends on the lithology. Thus proper knowledge of the lithology of the study area is required in order to obtain representative result of the heat flow values. The pre-rift rocks surrounding the Malawi rift is characterized by Precambrian crystalline metamorphic and igneous rocks and Paleozoic-Mesozoic sedimentary rocks [*Carter and Bennett*, 1973*; Chilton and Smith-Carington*, 1984]. The geologic map of Malawi of Malawi suggests that Malawi Precambrian basement complex is dominated by gneisses, granulite, and schists. Based on this an average thermal conductivity value of 2.9 $Wm^{-1}K^{-1}$ was used in this study. This value is within the general range of thermal conductivities (2.5–5.0 $Wm^{-1}K^{-1}$) for metamorphic rocks [*Lillie*, 1999*; Chilton and Smith-Carington*, 1984].

CHAPTER IV

RESULTS

4.1. Depths to Moho

The Moho depth estimates range between 31 and 45 km (Figure 9). There is no consistent pattern of N-S elongated crustal thinning following the surface expression of the rift, with the crustal thickness varying between 35 and 39 km.

Figure 9 shows three regions of thick crust (40-45 km) beneath the Malawi Rift and surroundings. These include a region of thick crust beneath the RVP in the northern segment of the rift. Within the central part of the rift, a second region of thick crust extends beneath the Luangwa Rift Valley and the Niassa Craton and extends to the eastern flank of the Malawi Rift. This is the location where the rift bifurcates (see Figure 3). Further south, the third region of thick crust extends beneath the Mulanje Mountain. At this location the Malawi Rift changes its orientation from a generally N-S to NNE-SSW, extending on the western edge of the Mulanje Mountain.

Figure 9 also shows three regions of thin crust (31-34 km). This includes a NE-trending region of thin crust that extends beneath the Ruhuhu Trough. Within the central part of the rift, a second NE-trending region of thin crust extends beneath the Maniamba Trough. Further south, a third region of thin crust extends beneath the Zambezi Rift.

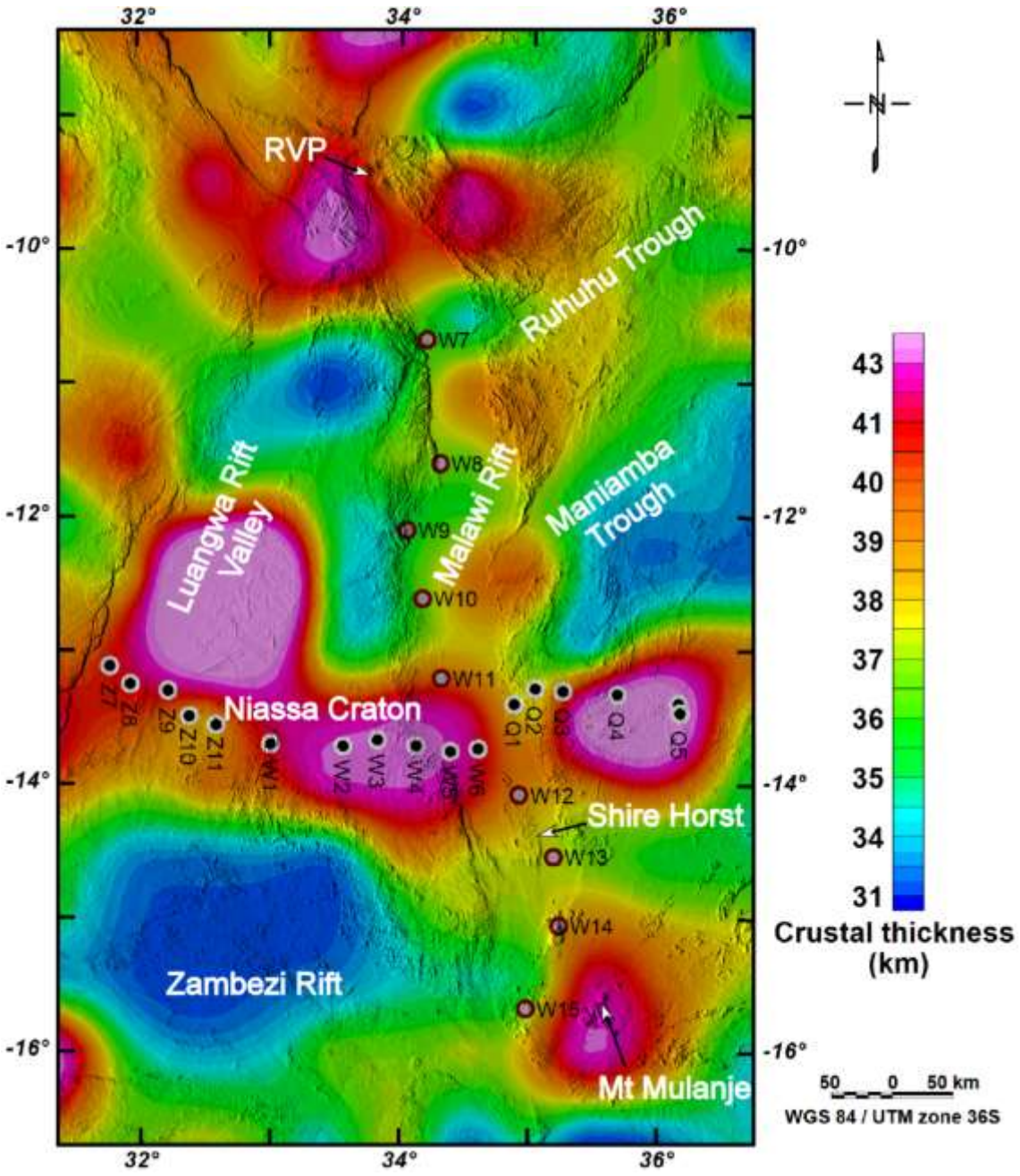

Figure 9. Map of the crustal thickness beneath the Malawi Rift and surroundings obtained from the two-dimensional (2D) radially averaged power spectrum analysis of the satellite gravity data in Figure 4. The crustal thickness map is draped onto Shuttle Radar Topography Mission (SRTM) Digital Elevation Model (DEM). The brown circles with gray infill labeled W7-W15 along strike the rift and the white circles with black infill labeled Z7-Q5 across the rift show locations of

passive seismic stations for the Seismic Arrays for African Rift Initiation (SAFARI) [*Gao et al.*, 2013]. Stations labeling is adopted from the actual station ID's.

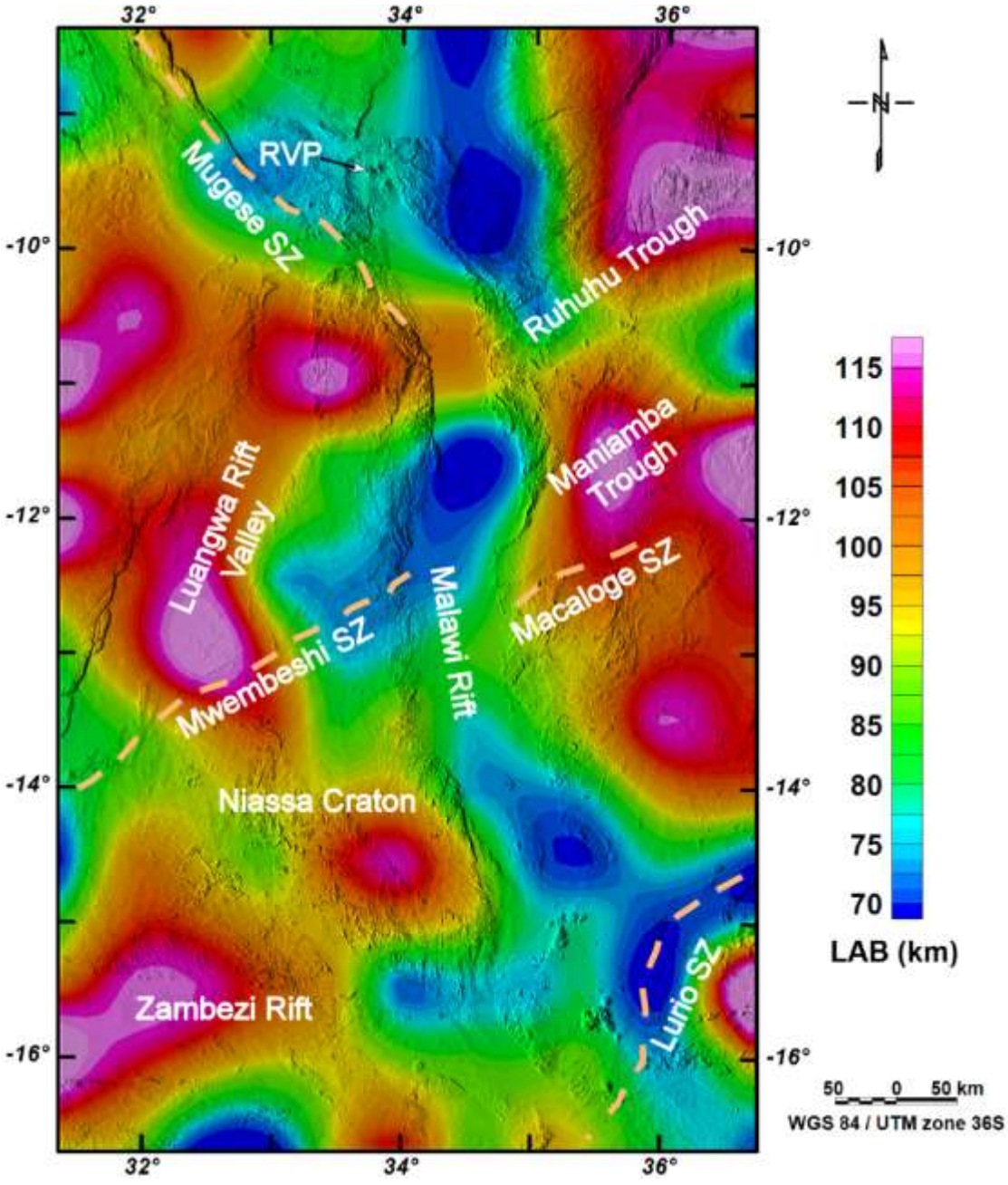

Figure 10. Map of the depth to the lithosphere-asthenosphere boundary (LAB) beneath the Malawi Rift and surroundings obtained from the two-dimensional (2D) radially averaged power spectrum analysis of the satellite gravity data in Figure 4. The lithospheric thickness map is

draped onto Shuttle Radar Topography Mission (SRTM) Digital Elevation Model (DEM). Dotted brown lines represent shear zones (SZ).

4.2. Depth to the lithosphere-asthenosphere boundary

Estimates of the depth to the LAB beneath the Malawi Rift and surroundings range from 64 to 124 km (Figure 10). Different from the crustal thickness heterogeneity, in general, an elevated LAB is found to underlie the entire length of the rift stretching from its northern to southern tips. The depth of this density-contrast boundary is as shallow as ~64 km beneath the rift and it is deeper than 100 km beneath the Precambrian terranes reaching in places ~124 km. Where Precambrian shear zones meet the rift, the elevated LAB tends to align with the shear zones where shallower LAB is observed.

4.3. Curie point depth and heat flow

The CPD values beneath the Malawi Rift and surroundings range between 18 and 27 km (Figure 11) while the heat flow values range between 59 and 81 mWm^{-2} (Figure 12). There is a NE-trending zone of elevated CPD (18-20 km) and high heat flow (70-81 mWm^{-2}) that extends beneath the rift center, to the Ruhuhu and Maniamba troughs. Moreover, there is a localized region of high heat flow (70-81 mWm^{-2}) beneath the RVP. Further south, there is another E-W trending region of high heat flow (70-81 mWm^{-2}) that extends beneath the Shire Graben and the Zambezi Rift. Apart from the thermal anomaly beneath the RVP, regions of high heat flow are coincident with the Karoo-aged rift basins.

Figure 12 also shows two regions of relatively lower (59-63 mWm^{-2}) heat flow. This includes an E-W trending region of lower (59-63 mWm^{-2}) heat flow values that extends beneath the Bangweulu Block to the western flank of the northern segment of the Malawi Rift.

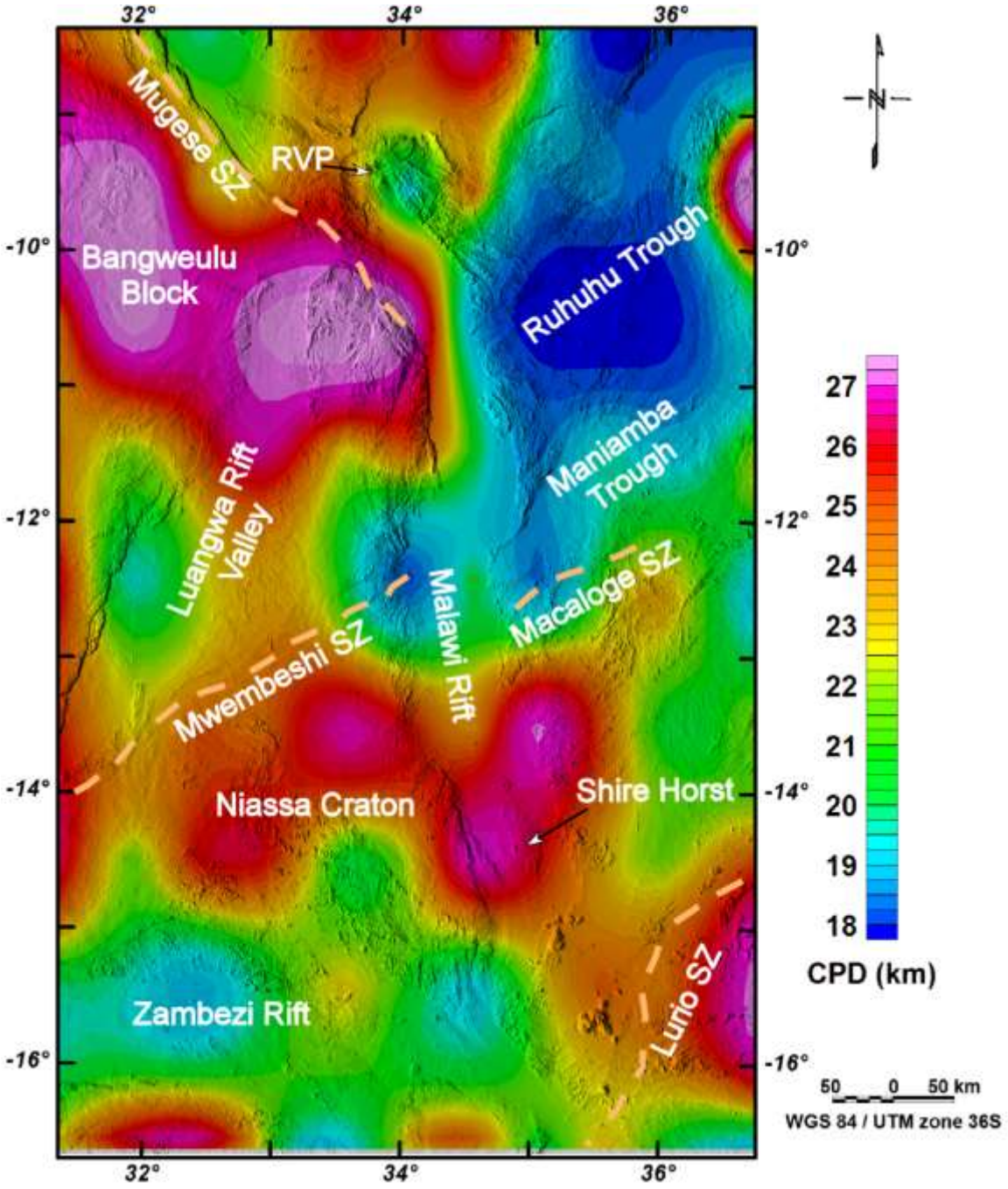

Figure 11. Map of the Curie Point Depth (CPD) values beneath the Malawi Rift and surroundings obtained from two-dimensional (2D) radially averaged power spectrum analysis of the aeromagnetic data in Figure 7. The CPD map is draped onto Shuttle Radar Topography Mission (SRTM) Digital Elevation Model (DEM). Dotted brown lines represent shear zones (SZ).

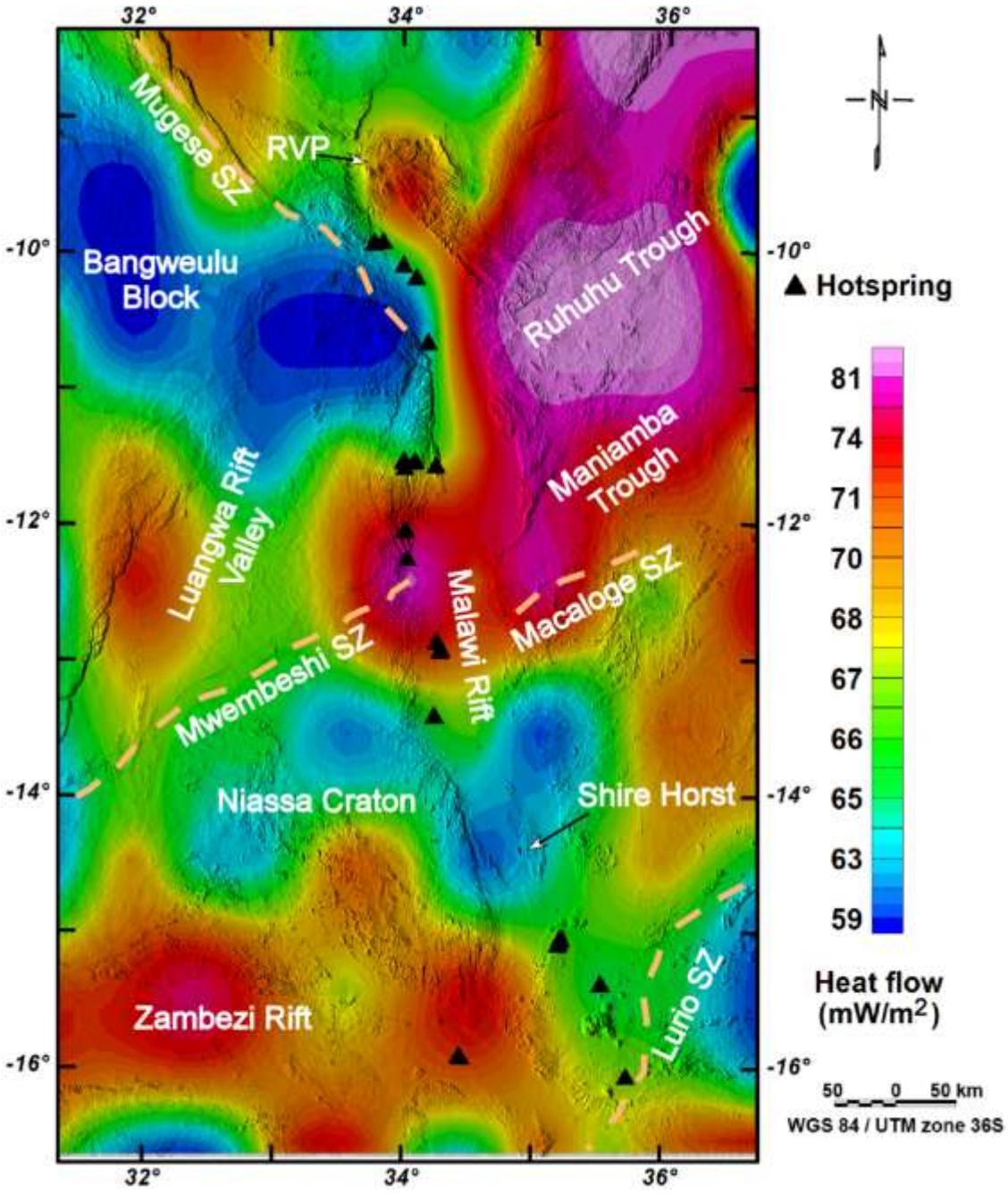

Figure 12. Map of the heat flow beneath the Malawi Rift and surroundings calculated from the Curie Point Depth (CPD) values which are obtained from the two-dimensional (2D) radially averaged power spectrum analysis of the aeromagnetic data in Figure 5. The heat flow map is draped onto Shuttle Radar Topography Mission (SRTM) Digital Elevation Model (DEM). The

black triangles are hot spring locations from *Atekwana et al.* [2015]. Dotted brown lines represent shear zones (SZ).

Within the central part of the rift, another E-W trending region of lower (59-63 mWm^{-2}) heat flow is found extending from beneath the Niassa Craton to the Shire Horst, where the rift bifurcates (see Figure 3).

CHAPTER V

DISCUSSION

5.1. Role of pre-existing lithospheric heterogeneity on the lithospheric and thermal structures of the Malawi Rift

The crustal thickness and heat flow estimates for the Malawi Rift are in general good agreement with those reported from the Okavango Rift Zone and other segments of the Western Branch of the EARS such as the Kivu Rift, and the Tanganyika Rifts (Figure 1) were crustal thickness ranging between 30 and 45 km [*Tuluka,* 2010; *Leseane et al.,* 2015] and heat flow between 53 and 82 mWm^{-2} [*Fadaie and Ranalli,* 1990; *Leseane et al.,* 2015] are reported. Generally, continental rifts are characterized by surface manifestation in the form of elongated grabens, crustal thinning, and elevated heat flow. Even the world's youngest continental rift (Okavango Rift Zone in Botswana) shows Moho shallowing of 4-5 km beneath the rift axis [*Yu et al.,* 2015] coincident with an elevated heat flow (>55 mWm^{-2}) [*Leseane et al.,* 2015]. However, results of this work do not show such consistent crustal thinning and elevated heat flow beneath the axis of the Malawi Rift. Instead regions of thin crust (31-34 km) and elevated heat flow (70-81 mWm^{-2}) occur beneath the surrounding Paleozoic-Mesozoic Karoo-aged Ruhuhu and Maniamba troughs and the Zambezi Rift. The high heat flow (70-81 mWm^{-2}) at the rift center is consistent with earlier observations by *Von Herzen and Vacquier,* [1967] with a mean value of 82 ± 78 mWm^{-2} after being corrected for lake sediment blanketing, and lake circulation [*Fadaie and Ranalli,*

1990].The elevated heat flow at the rift center is correlated to the presence of hot springs with temperature reaching 79.3^{0}C (black triangles in Figure 12) [*Gondwe et al.,* 2012*; Atekwana et al.,* 2015*; Kaonga et al.,* 2014]. However, *O'Donnell et al.* [2013] through Rayleigh wave tomography determined pronounced velocity lows at depths as shallow as 68 km beneath the RVP and at the southern end of Lake Malawi, but not beneath the central portion of the lake. This suggest that the thermal anomaly at the rift center is confined to a shallow depth within the crust and not related to the rifting process. This is corroborated by geochemical analyses of hot springs around the rift center which show no geochemical signature indicative of interaction of surface water with a deep heat source such as a mantle melt [*Atekwana et al.,* 2015]. Considering that the thermal anomaly at the rift center is not related to the rifting process, this work suggest an alternative explanation in which this thermal anomaly is considered to be related to the NE-trending Karoo-aged Ruhuhu and Maniamba troughs.

Since lithospheric thermal perturbations diminishes with time, elevated heat flow anomalies associated with rifting are measured only in Cenozoic rifts [*Morgan,* 1983]. Thus the high heat flow beneath the Karoo-aged Ruhuhu and Maniamba troughs and the Zambezi Rift must be due to uranium mineralization in these sedimentary basin. This is supported by the current mining of uranium that is hosted by Karoo sedimentary rocks including those of the Ruhuhu Trough in southern Tanzania. Thus except for the thermal anomaly beneath the RVP, there is no current thermal perturbation beneath the Malawi Rift that can be interpreted as associated with the rifting processes.

The variability in the crustal thickness and heat flow values estimates are reflective of the different tectonic elements highlighting the importance of tectonic inheritance in the crustal and thermal structures beneath the Malawi Rift. It is documented that several tectonic and magmatic events have modified the lithosphere beneath the Malawi Rift and surroundings before the

Neogene rifting processes since as early as the Precambrian. (1) The observed thick and cold crust (40-45 km and 59-63 mWm^{-2}) beneath the Niassa Craton might have been established since the pre-Mesoproterozoic (~1500 Ma) [*Andreoli,* 1984; *Daly*, 1986; *De Waele et al.,* 2006]. (2) The thin (31-34 km) and hot (70-81 mWm^{-2}) crust beneath the Ruhuhu and Maniamba troughs and the Zambezi and Shire Graben formed during the Paleozoic-Mesozoic Karoo-rifting events, during the breakup of Gondwana in the late Carboniferous to early Jurassic (~300 to ~200 Ma) [*Banks et al.,* 1995]. (3) The thick crust (40-45 km) beneath the RVP and the Mulanje Mountain (Figure 8) are probably due to magma-underplating events during the Neogene and Upper Jurasic to Cretaceous. The Mulanje Mountain is made-up of Upper Jurassic to Cretaceous (~150 to ~100 Ma) igneous intrusions [*Platt and Wooley*, 1986]. Its formation is concomitant with the emplacement of the ring complexes in southern Malawi [*Platt and Wooley*, 1986]. Thus the thick crust beneath the Mulanje Mountain is inherited since the Upper Jurassic to Cretaceous (~145 Ma) alkaline igneous activity in Malawi. While there is elevated heat flow within the Neogene RVP (Figure 12), the thermal anomaly due to the underplated magmatic body associated with the Mulanje Mountain must have completely dissipated.

Different from the crustal thickness heterogeneity, Figure 10 indicates a localized zone of SCLM thinning from 124 km away from the rift to ~64 km beneath the entire length of the rift stretching from its northern to southern tips. This suggests that the extensional strain of the lithosphere due to the Neogene rifting processes in Malawi is preferentially localized in the SCLM than in the crust. SCLM thinning extends beneath the Livingstone Mountain adjacent to the Livingstone Fault (Figure 3). This thinning may be responsible for the uplift of the Livingstone Mountain to its present-day elevation (up to ~ 2700 m). Using 3D gravity modeling, a similar uniform thinning of the SCLM (from 140 to < 45 km) was inferred beneath the Alboran Basin, west Mediterranean [*Torne et al.,* 2000].

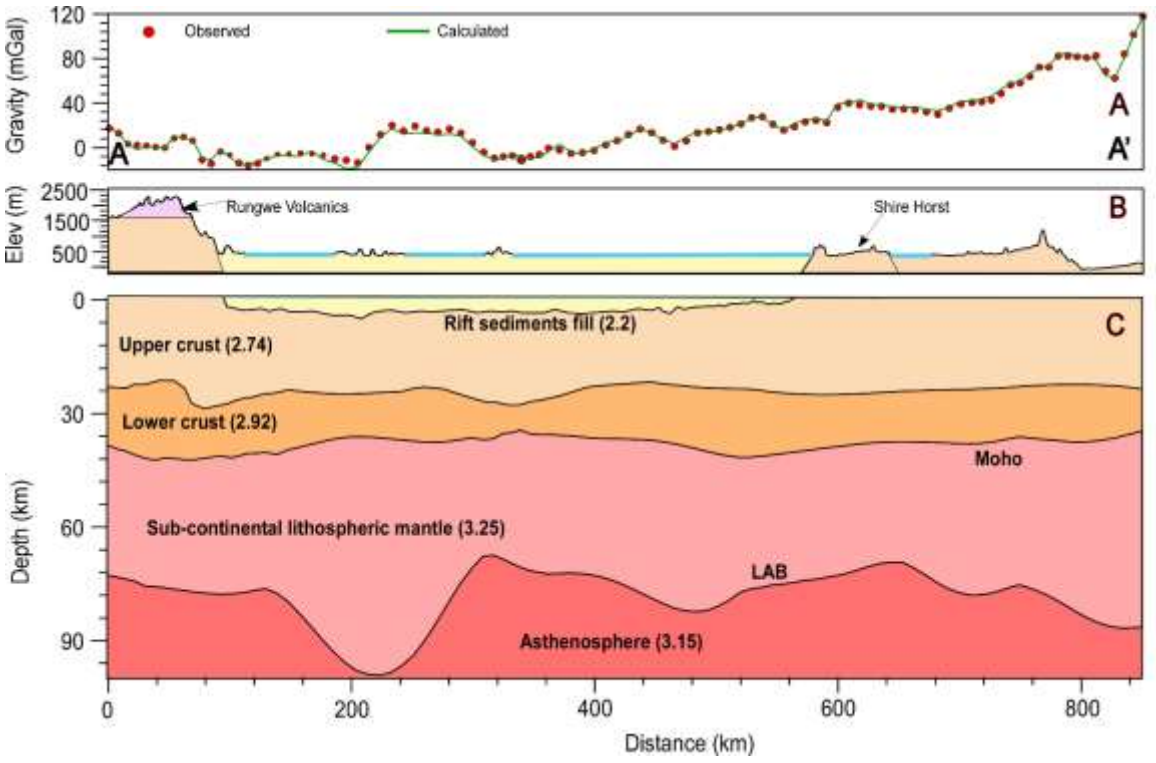

Figure 13. (A) Observed (Red circles) and calculated (Green lines) Bouguer gravity anomalies along strike the Malawi Rift following profile A-A'. The calculated Bouguer gravity anomaly represents the best fit for the two-dimensional (2D) forward gravity model in figure 13C. (B) An idealized geological cross-section of the Malawi Rift and the surroundings along profile A-A'. (C) A 2D forward gravity model showing the lithospheric structure beneath the strike of the Malawi Rift. Numbers in parentheses are densities in g/cm^3. LAB = lithosphere-asthenosphere boundary. See Figure 4 for location of the profile.

5.2. Decoupling of the crust from the Sub-continental lithospheric mantle

This study used 2D forward modeling of the satellite gravity data along profiles A-A', B-B' and C-C' (Figure 4) to reconcile the observed lithospheric structure of the Malawi Rift. Profiles A-A' and C-C' cut across locations of passive seismic stations of the Seismic Arrays for African Rift Initiation (SAFARI) [*Gao et al.,* 2013]. This permits future comparison of the results from this

study to the lithospheric structure yet to be derived from passive seismic studies. Gravity models suffer from non-uniqueness and in order to construct meaningful geological models, constraints such as rock densities, thickness and lateral variations of rock units must be used. Because these constraints are not readily available in the Malawi Rift and surrounding areas, estimates of the depth to Moho and LAB obtained from the 2D radially averaged power spectrum method were used as initial constraints in the first iteration of the 2D forward modeling of the satellite gravity data. The thickness and densities of the upper crust (2.76 g/cm^3), the lower crust (2.92 g/cm^3) and the SCLM (3.25 g/cm^3), were estimated from gravity and seismic studies of different parts of the EARS [e.g., *Mahatsente et al.*, 1999; *Simiyu and Keller*, 2001; *Mickus* et al., 2007; *Leseane et al.*, 2015]. The final gravity model was determined by varying the initial crustal thickness and depth to LAB by ~10%, and the initial densities by ~15%.

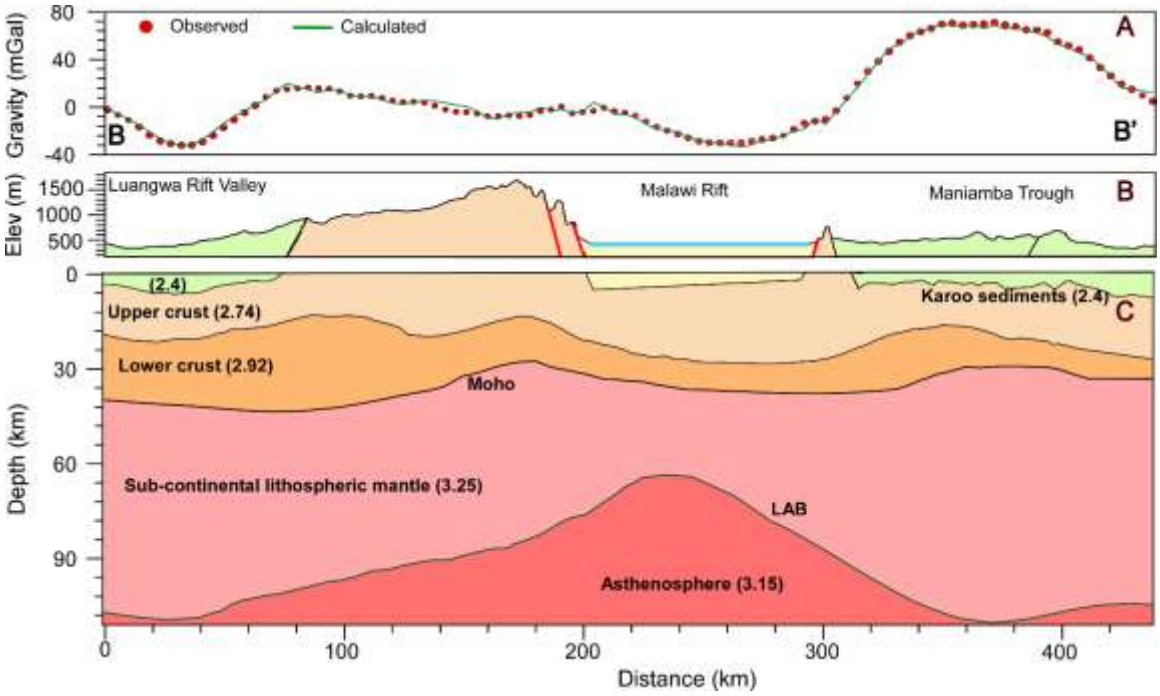

Figure 14. (A) Observed (Red circles) and calculated (Green line) Bouguer gravity anomalies across the Malawi Rift. The calculated Bouguer gravity anomaly represents the best fit for the two-dimensional (2D) forward gravity model in figure 14C. (B) An idealized geological cross

section of the Malawi Rift and surrounding structures along profile B-B'. (C) A 2D forward gravity model showing the lithospheric structure beneath the Malawi Rift along profile B-B'. Numbers in parentheses are densities in g/cm^3. LAB = lithosphere-asthenosphere boundary. See Figure 4 for location of the profile.

The important points to note from the 2D forward models include: (a) Along profile A-A' the lithospheric structure (Figure 13) is characterized by a relatively flat Moho with slight undulations along the N-S strike of the Malawi Rift, while the SCLM experience significant thinning. (b) Across the rift center, the lithospheric structure beneath profile B-B' (Figure 14), shows: (1) Significant stretching of the lower crust beneath the rift. (2) Elevated asthenosphere where the lab is as shallow as ~64 km. (3) The surface expression of the rift (see Figure 14B) coincides to where the rift is widest (80 km). (c) Further south of the Malawi Rift, the lithospheric structure beneath profile C-C' (Figure 15), shows: (1) a thicker or less stretched lower crust, (2) The asthenosphere is deeper (~ 80 km), and (3) the surface expression of the rift (see Figure 15B) is narrower (55 km).

The significant stretching of the lower crust at the rift center, and the observation that the asthenosphere is shallower suggest that the lower crust at the rift center is hotter and more ductile, while further south, the lower crust become colder and more viscous. This is consistent with preliminary results of passive seismic studies in the Malawi Rift [*Yu et al.,* 2013], which suggest V_p/V_s ratios of 1.68 at the rift center and a value of 1.84 further south. The V_p/V_s ratio of 1.84 translates to a Poisson's ratio of 0.29 indicating a lower crust of mafic composition giving it strength to support brittle deformation. This provides explanation for the deep earthquakes (>30 km) recorded in southern Malawi, due to the rupture of the Bilila-Mtakataka Fault (Figure 3) in a single large magnitude seismic event [*Jackson and Blenkinsop,* 1997].

Figures 13, 14 and 15 suggest that there is heterogeneous thinning of the crust and consistent thinning of the SCLM by a factor of 1.5 to 1.8 beneath the Malawi Rift and surroundings. The heterogeneous thinning of the crust is inherited from the pre-existing lithospheric stretching events suggesting that the Neogene rifting process in Malawi did not significantly alter the crustal structure. However, the uniform thinning of the SCLM following the surface expression of the Malawi Rift suggests that extensional strain of the lithosphere during the Miocene rifting processes in Malawi was preferentially localized in the SCLM. Further research is required to decipher the mechanism for the uniform thinning of the SCLM beneath the Malawi Rift.

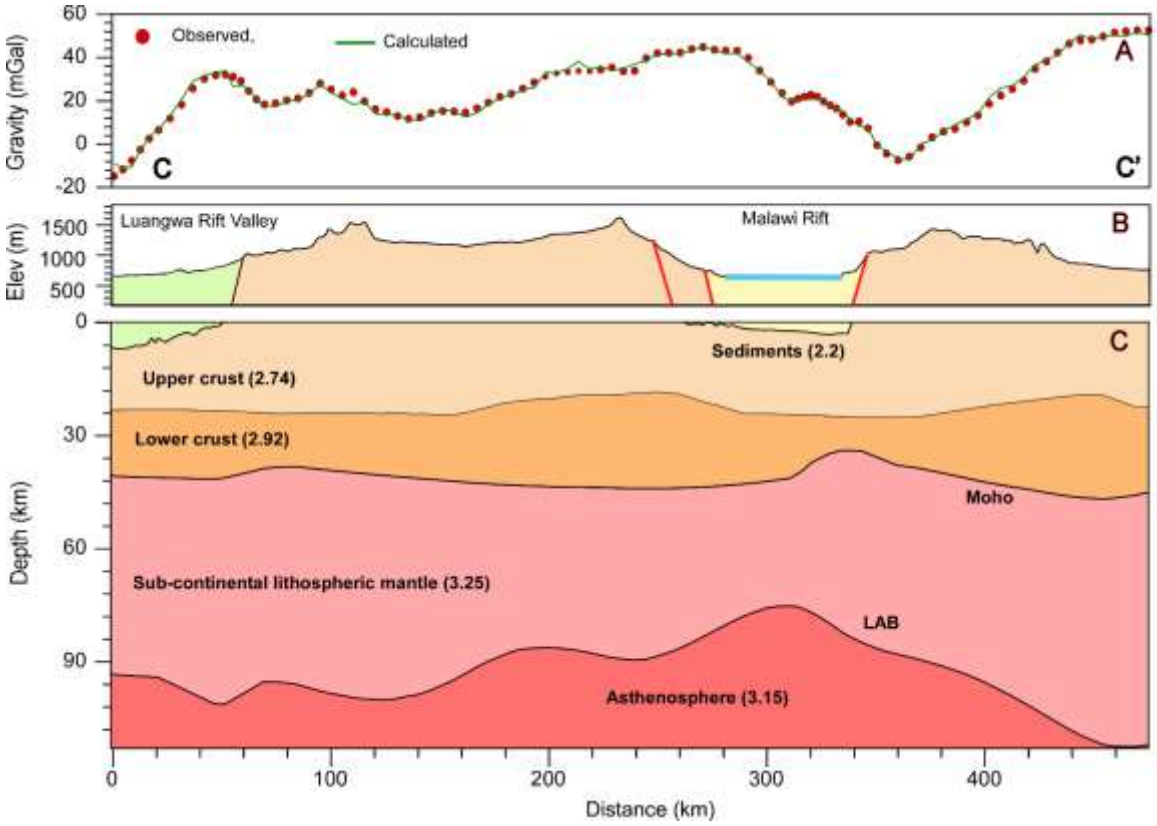

Figure 15. (A) Observed (Red circles) and calculated (Green line) Bouguer gravity anomalies across the Malawi Rift along profile C-C'. The calculated Bouguer gravity anomaly represents the best fit for the two-dimensional (2D) forward gravity model in figure 15C. (B) An idealized geological cross-section of the Malawi Rift and surroundings along profile C-C'. (C) A 2D

forward gravity model showing the lithospheric structure beneath the Malawi Rift along profile C-C'. Numbers in parentheses are densities in g/cm^3. LAB = lithosphere-asthenosphere boundary. See Figure 4 for location of the profile.

The tectonic implication is that the crust is decoupled from the SCLM during the evolution of the Malawi Rift. Decoupling of the crust and the SCLM during continental rifting has been previously suggested [e.g., *Hopper and Buck,* 1998; *Gasper-Escribano*, 2003]. The rheological stratification of the lithosphere suggest a relatively ductile lower crust sandwiched between a brittle upper crust and the uppermost part of the SCLM. Decoupling is the mutually independent response of the various lithospheric layers to the rifting process [*Hopper and Buck*, 1998]. Several styles of extensional decoupling of the crust from the SCLM have been proposed and summarized by *Gasper-Escribano,* [2003]. These include: (1) Vertical or diffuse decoupling of the crust from the SCLM which occurs where the lower crust is viscous and isotropic and will not transmit shear stresses from below but will flow horizontally to compensate isostatic equilibrium [*Handy et al.,* 2005]. This is suggested to be a characteristic of wide rifts such as Basin and Range [*Buck,* 1991]. (2) Horizontal or shear decoupling that includes lateral movement of the crust relative to the SCLM, interacting mechanically by shearing in the intermediate weak layer (Moho) facilitating differential stretching [*Hopper and Buck,* 1996]. (3) Partial decoupling which is a combination of vertical and horizontal decoupling that occurs when the viscosity of the lower crust is not low enough to produce significant lateral flow to accommodate all load unbalances [*Ter Voorde et al.,* 1998]. On the other hand, coupling occurs where the lithosphere deforms as a whole without intermediate layering [*Janssen et al.,* 1993]. Results of this work thus show vertical or diffused decoupling at the rift center but partial decoupling in the southern part of the Malawi Rift.

5.3. Implications of decoupling on the development of the Malawi Rift

The above results show that the ductile lower crust plays a dominant role in defining the modes of continental rifting. Given that the more stretched (more ductile) lower crust at the rift center (Figure 14) is coincident with where the rift is widest, further suggest an import role of the ductile deformation of the lower crust in the development of the Malawi Rift. *Schueller et al.* [2005, 2010] have shown through numerical modeling that the viscosity of ductile layers in brittle–ductile systems controls the numbers of faults (and thus the width of the rift) in brittle layers, defining the brittle–ductile coupling. (1) When the crust and SCLM are vertically decoupled (with a more ductile lower crust), significant stretching of the lower crust engenders new faults in the upper crust to accommodate the displacement rate producing a wider rift. (2) When the crust and SCLM are partially decoupled (stronger lower crust), limited stretching of the lower crust will also yield localized faulting (rift is narrower) in the upper crust to accommodate the displacement rate.

CHAPTER VI

CONCLUSIONS

The lithospheric structure, and thermal structure determined from 2D radially averaged power spectrum analysis and 2D forward modeling of the lithospheric structure beneath the Malawi Rift and surroundings allow reaching the following conclusions:

(1) Neogene rifting did not greatly modify the crustal thickness beneath the Malawi Rift. Instead, the Malawi Rift inherited a heterogeneous crustal thickness, from the pre-existing lithospheric stretching events.

(2) Unlike the crustal thickness heterogeneity, thinning of the SCLM is more uniform beneath the Malawi Rift and follows the surface expression of the rift, suggesting this thinning is related to the Neogene rifting in Malawi.

(3) Apart from the thermal anomaly beneath the RVP, there is no observed thermal anomaly related to the Neogene rifting in Malawi.

(4) The extensional strain of the lithosphere is preferentially localized in the SCLM, suggesting decoupling of the crust from the SCLM during the development of the Malawi Rift.

(5) Comparing observations from this study in the central and southern parts of the Malawi Rift with established theoretical styles of crust-SCLM decoupling suggest that the central part of the rift is characterized by vertical decoupling where the lower crust is viscous

and isotropic and will not transmit shear stresses from heat below but will flow horizontally to compensate isostatic equilibrium. Differently, the southern part of the rift is characterized by partial decoupling which occurs when the viscosity of the lower crust is not low enough to produce significant lateral flow to accommodate all load unbalances.

(6) Different from previous proposition that crust-SCLM decoupling lead to the formation of wide rifts, this work show for the first time that decoupling can be associated with narrow rifts given that, they are formed with a heterogeneous lithosphere with pre-existing tectonic fabrics that are present at high angle to the rift strike.

REFERENCES

Aboud, E., A. Salem, and M. Mekkawi (2011), Curie depth map for Sinai Peninsula, Egypt deduced from the analysis of magnetic data, *Tectonophysics*, *506*(1), 46-54.

Arnaiz-Rodríguez, M. S., and N. Orihuela (2013), Curie point depth in Venezuela and the Eastern Caribbean, *Tectonophysics*, *590*, 38-51.

Atekwana, E. (2015), Chemical and isotopic characteristics of hot springs along the along the Neogene Malawi rift, paper presented at 2015 AGU Fall Meeting, Agu.

Balmino, G., N. Vales, S. Bonvalot, and A. Briais (2012), Spherical harmonic modelling to ultra-high degree of Bouguer and isostatic anomalies, *Journal of Geodesy*, *86*(7), 499-520.

Banks, N., K. Bardwell, and S. Musiwa (1995), Karoo rift basins of the Luangwa Valley, Zambia, *Geological Society, London, Special Publications*, *80*(1), 285-295.

Betzler, C., and U. Ring (1995), Sedimentology of the Malawi Rift: facies and stratigraphy of the Chiwondo Beds, northern Malawi, *Journal of Human Evolution*, *28*(1), 23-35.

Bhattacharyya, B., and L.-K. Leu (1975), Spectral analysis of gravity and magnetic anomalies due to two-dimensional structures, *Geophysics*, *40*(6), 993-1013.

Bianconi, F. (1987), Uranium geology of Tanzania, in *Uranium mineralization-new aspects on geology, mineralogy, geochemistry, and exploration methods*, edited.

Biggs, J., E. Nissen, T. Craig, J. Jackson, and D. Robinson (2010), Breaking up the hanging wall of a rift-border fault: The 2009 Karonga earthquakes, Malawi, *Geophysical Research Letters*, *37*(11).

Bingen, B., J. Jacobs, G. Viola, I. Henderson, Ø. Skår, R. Boyd, R. Thomas, A. Solli, R. Key, and E. Daudi (2009), Geochronology of the Precambrian crust in the Mozambique belt in NE Mozambique, and implications for Gondwana assembly, *Precambrian Research*, *170*(3), 231-255.

Blakely, R. J. (1988), Curie temperature isotherm analysis and tectonic implications of aeromagnetic data from Nevada, *Journal of Geophysical Research: Solid Earth*, *93*(B10), 11817-11832.

Bloomfield, K. (1966), 1: 1, 000,000 Geological map of Malawi, *Geol. Surv. Malawi*.

Bonvalot, S., G. Balmino, A. Briais, M. Kuhn, A. Peyrefitte, and N. Vales (2012), World Gravity Map, 636 1: 50,000,000 map, Eds*Rep.*, BGI-CGMW-CNES-IRD, Paris. 637.

Briggs, I. C. (1974), Machine contouring using minimum curvature, *Geophysics*, *39*(1), 39-48.

Buck, W. (2006), The role of magma in the development of the Afro-Arabian Rift System, *Geological Society, London, Special Publications*, *259*(1), 43-54.

Buck, W. R. (1991), Modes of continental lithospheric extension, *Journal of Geophysical Research*, *96*(B12), 20,161-120,178.

Calais, E., C. Ebinger, C. Hartnady, and J. Nocquet (2006), Kinematics of the East African Rift from GPS and earthquake slip vector data, *Special Publication-Geological Society of London*, *259*, 9.

Carter, G., and J. D. Bennett (1973), Geology and Mineral Resources of Malawi, *Malawi, Geol. Surv. Dep., Bull., 1973, 6, 1-62.*

Casey, M., C. Ebinger, D. Keir, R. Gloaguen, and F. Mohamed (2006), Strain accommodation in transitional rifts: extension by magma intrusion and faulting in Ethiopian rift magmatic segments, *Geological Society, London, Special Publications*, *259*(1), 143-163.

Castaing, C. (1991), Post-Pan-African tectonic evolution of South Malawi in relation to the Karroo and recent East African rift systems, *Tectonophysics*, *191*(1), 55-73.

Chilton, P., and A. Smith-Carington (1984), *Characteristics of the weathered basement aquifer in Malawi in relation to rural water supplies*, IAHS Press.

Chorowicz, J. (2005), The East African rift system, *Journal of African Earth Sciences*, *43*(1), 379-410.

Chorowicz, J., and C. Sorlien (1992), Oblique extensional tectonics in the Malawi Rift, Africa, *Geological Society of America Bulletin*, *104*(8), 1015-1023.

Cohen, A. S., M. J. Soreghan, and C. A. Scholz (1993), Estimating the age of formation of lakes: an example from Lake Tanganyika, East African Rift system, *Geology*, *21*(6), 511-514.

Contreras, J., M. H. Anders, and C. H. Scholz (2000), Growth of a normal fault system: observations from the Lake Malawi basin of the east African rift, *Journal of Structural Geology*, *22*(2), 159-168.

Craig, T., J. Jackson, K. Priestley, and D. McKenzie (2011), Earthquake distribution patterns in Africa: their relationship to variations in lithospheric and geological structure, and their rheological implications, *Geophysical Journal International*, *185*(1), 403-434.

Daly, M., J. Chorowicz, and J. Fairhead (1989), Rift basin evolution in Africa: the influence of reactivated steep basement shear zones, *Geological Society, London, Special Publications*, *44*(1), 309-334.

De Waele, B., A. Kampunzu, B. Mapani, and F. Tembo (2006), The Mesoproterozoic Irumide belt of Zambia, *Journal of African Earth Sciences*, *46*(1), 36-70.

Ebinger, C., A. Ayele, D. Keir, J. Rowland, G. Yirgu, T. Wright, M. Belachew, and I. Hamling (2010), Length and timescales of rift faulting and magma intrusion: the Afar rifting cycle from 2005 to present, *Annual Review of Earth and Planetary Sciences*, *38*, 439-466.

Ebinger, C., and M. Casey (2001), Continental breakup in magmatic provinces: An Ethiopian example, *Geology*, *29*(6), 527-530.

Ebinger, C., A. Deino, R. Drake, and A. Tesha (1989), Chronology of volcanism and rift basin propagation- Rungwe volcanic province, East Africa, *Journal of Geophysical Research*, *94*(11), 15785-15803.

Ebinger, C., A. Deino, A. Tesha, T. Becker, and U. Ring (1993), Tectonic controls on rift basin morphology: evolution of the Northern Malawi (Nyasa) Rift, *Journal of Geophysical Research: Solid Earth*, *98*(B10), 17821-17836.

Ebinger, C. J., B. Rosendahl, and D. Reynolds (1987), Tectonic model of the Malaŵi rift, Africa, *Tectonophysics*, *141*(1), 215-235.

Fadaie, K. t., and G. Ranalli (1990), Rheology of the lithosphere in the East African Rift System, *Geophysical Journal International*, *102*(2), 445-453.

Fagereng, Å. (2013), Fault segmentation, deep rift earthquakes and crustal rheology: Insights from the 2009 Karonga sequence and seismicity in the Rukwa–Malawi rift zone, *Tectonophysics*, *601*, 216-225.

Fairhead, J., and C. Okereke (1987), A regional gravity study of the West African rift system in Nigeria and Cameroon and its tectonic interpretation, *Tectonophysics*, *143*(1-3), 141-159.

Flannery, J., and B. Rosendahl (1990), The seismic stratigraphy of Lake Malawi, Africa: implications for interpreting geological processes in lacustrine rifts, *Journal of African Earth Sciences (and the Middle East)*, *10*(3), 519-548.

Fritz, H., M. Abdelsalam, K. Ali, B. Bingen, A. Collins, A. Fowler, W. Ghebreab, C. Hauzenberger, P. Johnson, and T. Kusky (2013), Orogen styles in the East African Orogen: a review of the Neoproterozoic to Cambrian tectonic evolution, *Journal of African Earth Sciences*, *86*, 65-106.

Fullea, J., M. Fernàndez, J. C. Afonso, J. Vergés, and H. Zeyen (2010), The structure and evolution of the lithosphere–asthenosphere boundary beneath the Atlantic–Mediterranean Transition Region, *Lithos*, *120*(1), 74-95.

Gao, S. S., K. H. Liu, C. A. Reed, Y. Yu, B. Massinque, H. Mdala, M. Moidaki, D. Mutamina, E. A. Atekwana, and S. Ingate (2013), Seismic arrays to study African rift initiation, *Eos, Transactions American Geophysical Union*, *94*(24), 213-214.

Gaspar-Escribano, J., M. Ter Voorde, E. Roca, and S. Cloetingh (2003), Mechanical (de-) coupling of the lithosphere in the Valencia Trough (NW Mediterranean): what does it mean?, *Earth and Planetary Science Letters*, *210*(1), 291-303.

Gómez-Ortiz, D., B. Agarwal, R. Tejero, and J. Ruiz (2011), Crustal structure from gravity signatures in the Iberian Peninsula, *Geological Society of America Bulletin*, *123*(7-8), 1247-1257.

Gómez-Ortiz, D., R. Tejero-López, R. Babín-Vich, and A. Rivas-Ponce (2005), Crustal density structure in the Spanish Central System derived from gravity data analysis (Central Spain), *Tectonophysics*, *403*(1), 131-149.

Gondwe, K., A. Allen, L. Georgsson, U. Loga, and G. Tsokonombwe (2012), Geothermal development in Malawi-a country update, paper presented at 4th African rift geothermal conference. Geothermal solutions to Africa's energy needs, UN Gigiri complex, Nairobi, Kenya, Nairobi.

Gueydan, F., C. Morency, and J.-P. Brun (2008), Continental rifting as a function of lithosphere mantle strength, *Tectonophysics*, *460*(1), 83-93.

Handy, M., J. Babist, R. Wagner, C. Rosenberg, and M. Konrad (2005), Decoupling and its relation to strain partitioning in continental lithosphere: insight from the Periadriatic fault system (European Alps), *Geological Society, London, Special Publications*, *243*(1), 249-276.

Hanson, R. E., T. J. Wilson, and H. Munyanyiwa (1994), Geologic evolution of the Neoproterozoic Zambezi orogenic belt in Zambia, *Journal of African Earth Sciences*, *18*(2), 135-150.

Hargrove, U. S., R. E. Hanson, M. W. Martin, T. G. Blenkinsop, S. A. Bowring, N. Walker, and H. Munyanyiwa (2003), Tectonic evolution of the Zambezi orogenic belt: geochronological, structural, and petrological constraints from northern Zimbabwe, *Precambrian Research*, *123*(2), 159-186.

Hopper, J. R., and W. R. Buck (1996), and passive margin formation, *Journal of Geophysical Research*, *101*(B9), 20,175-120,194.

Hopper, J. R., and W. R. Buck (1998), Styles of extensional decoupling, *Geology*, *26*(8), 699-702.

Hunt, C. P., B. M. Moskowitz, and S. K. Banerjee (1995), Magnetic properties of rocks and minerals, *Rock physics & phase relations: a handbook of physical constants*, 189-204.

Hussein, M., K. Mickus, and L. F. Serpa (2013), Curie point depth estimates from aeromagnetic data from Death Valley and surrounding regions, California, *Pure and Applied Geophysics*, *170*(4), 617-632.

Jackson, J., and T. Blenkinsop (1997), The Bilila-Mtakataka fault in Malaŵi: An active, 100-km long, normal fault segment in thick seismogenic crust, *Tectonics*, *16*(1), 137-150.

Janssen, M., M. Torné, S. Cloetingh, and E. Banda (1993), Pliocene uplift of the eastern Iberian margin: Inferences from quantitative modelling of the Valencia Trough, *Earth and Planetary Science Letters*, *119*(4), 585-597.

Kaonga, H., G. Tsokonombwe, and T. Kamanga Status of Geothermal Exploration in Malawi.

Katumwehe, A. B., M. G. Abdelsalam, and E. A. Atekwana (2015), The role of pre-existing Precambrian structures in rift evolution: The Albertine and Rhino grabens, Uganda, *Tectonophysics*, *646*, 117-129.

Kreuser, T., H. Wopfner, C. Kaaya, S. Markwort, P. Semkiwa, and P. Aslandis (1990), Depositional evolution of Permo-Triassic Karoo basins in Tanzania with reference to their economic potential, *Journal of African Earth Sciences (and the Middle East)*, *10*(1-2), 151-167.

Laó-Dávila, D. A., H. S. Al-Salmi, M. G. Abdelsalam, and E. A. Atekwana (2015), Hierarchical segmentation of the Malawi Rift: The influence of inherited lithospheric heterogeneity and kinematics in the evolution of continental rifts, *Tectonics*, *34*(12), 2399-2417.

Leseane, K., E. A. Atekwana, K. L. Mickus, M. G. Abdelsalam, E. M. Shemang, and E. A. Atekwana (2015), Thermal perturbations beneath the incipient Okavango Rift Zone, northwest Botswana, *Journal of Geophysical Research: Solid Earth*, *120*(2), 1210-1228.

Lillie, R. J. (1999), *Whole earth geophysics*, Prentice Hall, New Jersey.

Mahatsente, R., G. Jentzsch, and T. Jahr (1999), Crustal structure of the Main Ethiopian Rift from gravity data: 3-dimensional modeling, *Tectonophysics*, *313*(4), 363-382.

Manea, M., and V. C. Manea (2011), Curie point depth estimates and correlation with subduction in Mexico, *Pure and applied geophysics*, *168*(8-9), 1489-1499.

Meert, J. G. (2003), A synopsis of events related to the assembly of eastern Gondwana, *Tectonophysics*, *362*(1), 1-40.

Mesko, G., C. Class, M. Maqway, N. Boniface, S. Manya, and S. Hemming (2014), The Timing of Early Magmatism and Extension in the Southern East African Rift: Tracking Geochemical Source Variability with 40Ar/39Ar Geochronology at the Rungwe Volcanic Province, SW Tanzania, paper presented at AGU Fall Meeting Abstracts.

Mickus, K., K. Tadesse, G. Keller, and B. Oluma (2007), Gravity analysis of the main Ethiopian rift, *Journal of African Earth Sciences*, *48*(2), 59-69.

Morgan, P. (1983), Constraints on rift thermal processes from heat flow and uplift, *Tectonophysics*, *94*(1), 277-298.

Mulibo, G. D., and A. A. Nyblade (2013), Mantle transition zone thinning beneath eastern Africa: Evidence for a whole-mantle superplume structure, *Geophysical Research Letters*, *40*(14), 3562-3566.

O'Donnell, J., A. Adams, A. Nyblade, G. Mulibo, and F. Tugume (2013), The uppermost mantle shear wave velocity structure of eastern Africa from Rayleigh wave tomography: constraints on rift evolution, *Geophysical Journal International*, ggt135.

Okubo, Y., R. Graf, R. Hansen, K. Ogawa, and H. Tsu (1985), Curie point depths of the island of Kyushu and surrounding areas, Japan, *Geophysics*, *50*(3), 481-494.

Olsen, K. H. (1995), *Continental Rifts: Evolution, Structure, Tectonics: Evolution, Structure, Tectonics*, Elsevier.

Platt, R. G., and A. R. Woolley (1986), The mafic mineralogy of the peralkaline syenites and granites of the Mulanje complex, Malawi, *Mineralogical Magazine*, *50*(355), 85-99.

Ring, U., and C. Betzler (1995), Geology of the Malawi Rift: kinematic and tectonosedimentary background to the Chiwondo Beds, northern Malawi, *Journal of Human Evolution*, *28*(1), 7-21.

Ring, U., C. Betzler, and D. Delvaux (1992), Normal vs. strike-slip faulting during rift development in East Africa: the Malawi rift, *Geology*, *20*(11), 1015-1018.

Ring, U., A. Kröner, R. Buchwaldt, T. Toulkeridis, and P. W. Layer (2002), Shear-zone patterns and eclogite-facies metamorphism in the Mozambique belt of northern Malawi, east-central Africa: implications for the assembly of Gondwana, *Precambrian Research*, *116*(1), 19-56.

Roberts, E. M., N. Stevens, P. O'connor, P. Dirks, M. D. Gottfried, W. Clyde, R. Armstrong, A. Kemp, and S. Hemming (2012), Initiation of the western branch of the East African Rift coeval with the eastern branch, *Nature Geoscience*, *5*(4), 289-294.

Ross, H. E., R. J. Blakely, and M. D. Zoback (2006), Testing the use of aeromagnetic data for the determination of Curie depth in California, *Geophysics*, *71*(5), L51-L59.

Russo, R., and e. R. Speed (1994), Spectral analysis of gravity anomalies and the architecture of tectonic wedging, NE Venezuela and Trinidad, *Tectonics*, *13*(3), 613-622.

Sacchi, R., P. Cadoppi, and M. Costa (2000), Pan-African reactivation of the Lurio segment of the Kibaran Belt system: a reappraisal from recent age determinations in northern Mozambique, *Journal of African Earth Sciences*, *30*(3), 629-639.

Saria, E., E. Calais, D. Stamps, D. Delvaux, and C. Hartnady (2014), Present-day kinematics of the East African Rift, *Journal of Geophysical Research: Solid Earth*, *119*(4), 3584-3600.

Schueller, S., F. Gueydan, and P. Davy (2005), Brittle-ductile coupling: Role of ductile viscosity on brittle fracturing, *Geophysical Research Letters*, *32*(10).

Schueller, S., F. Gueydan, and P. Davy (2010), Mechanics of the transition from localized to distributed fracturing in layered brittle–ductile systems, *Tectonophysics*, *484*(1), 48-59.

Shuey, R., D. Schellinger, A. Tripp, and L. Alley (1977), Curie depth determination from aeromagnetic spectra, *Geophysical Journal International*, *50*(1), 75-101.

Simiyu, S. M., and G. R. Keller (2001), An integrated geophysical analysis of the upper crust of the southern Kenya rift, *Geophysical Journal International*, *147*(3), 543-561.

Specht, T. D., and B. R. Rosendahl (1989), Architecture of the Lake Malawi rift, east Africa, *Journal of African Earth Sciences (and the Middle East)*, *8*(2), 355-382.

Spector, A., and F. Grant (1970), Statistical models for interpreting aeromagnetic data, *Geophysics*, *35*(2), 293-302.

Stamps, D. S., E. Calais, E. Saria, C. Hartnady, J. M. Nocquet, C. J. Ebinger, and R. M. Fernandes (2008), A kinematic model for the East African Rift, *Geophysical Research Letters*, *35*(5).

Tanaka, A., and Y. Ishikawa (2005), Crustal thermal regime inferred from magnetic anomaly data and its relationship to seismogenic layer thickness: The Japanese islands case study, *Physics of the Earth and Planetary Interiors*, *152*(4), 257-266.

Ter Voorde, M., R. Van Balen, G. Bertotti, and S. Cloetingh (1998), The influence of a stratified rheology on the flexural response of the lithosphere to (un) loading by extensional faulting, *Geophysical Journal International*, *134*(3), 721-735.

Thybo, H., and C. A. Nielsen (2009), Magma-compensated crustal thinning in continental rift zones, *Nature*, *457*(7231), 873-876.

Torne, M., M. Fernandez, M. Comas, and J. Soto (2000), Lithospheric structure beneath the Alboran Basin: results from 3D gravity modeling and tectonic relevance, *Journal of Geophysical Research: Solid Earth*, *105*(B2), 3209-3228.

Tselentis, G.-A., J. Drakopoulos, and K. Dimitriadis (1988), A spectral approach to moho depths estimation from gravity measurements in Epirus (NW Greece), *Journal of Physics of the Earth*, *36*(6), 255-266.

Tuluka, G. M. (2010), Crustal structure beneath two seismic broadband stations revealed from teleseismic P-wave receiver function analysis in the Virunga volcanic area, Western Rift Valley of Africa, *Journal of African Earth Sciences*, *58*(5), 820-828.

Von Herzen, R., and V. Vacquier (1967), Terrestrial heat flow in lake Malawi, Africa, *Journal of Geophysical Research*, *72*(16), 4221-4226.

Wölbern, I., G. Rümpker, K. Link, and F. Sodoudi (2012), Melt infiltration of the lower lithosphere beneath the Tanzania craton and the Albertine rift inferred from S receiver functions, *Geochemistry, Geophysics, Geosystems*, *13*(8).

Wright, T. J., C. Ebinger, J. Biggs, A. Ayele, G. Yirgu, D. Keir, and A. Stork (2006), Magma-maintained rift segmentation at continental rupture in the 2005 Afar dyking episode, *Nature*, *442*(7100), 291-294.

Yu, Y., K. H. Liu, C. A. Reed, M. Moidaki, K. Mickus, E. A. Atekwana, and S. S. Gao (2015), A joint receiver function and gravity study of crustal structure beneath the incipient Okavango Rift, Botswana, *Geophysical Research Letters*, *42*(20), 8398-8405.

APPENDIX

Data Management Plan

I. Types of Data

Satellite gravity data from the World Gravity Map 2012 (WGM12) was downloaded from the Bureau Gravimetrique International website. The aeromagnetic data were obtained from the Council of Geoscience, South Africa and include aeromagnetic data collected by the Government of Malawi between 1984 and 1985 through E-W transects with 1 km line spacing, 10 km tie lines, and 120 m terrain clearance.

II. Data and Metadata Standards

The WGM12 model comprises of surface gravity measurements (from land, airborne and marine surveys), and satellite gravimetry (from the GRACE mission). The Bouguer gravity data were computed using the spherical correction instead of the regular slab correction. The international geomagnetic reference field (IGRF) has been removed from the aeromagnetic data.

III. Policies for Access and Sharing

The satellite gravity data can be downloaded from http://bgi.omp.obs-mip.fr/data-products/Toolbox/WGM2012-maps-vizualisation-extraction. The aeromagnetic data can be acquired through the Geological Survey Department of Malawi.

Any researcher seeking to perform repeatability of this project's tasks or manipulate the data for other processing schemes not included in this project proposal may do so by accessing the data collected during this research study.

IV. Policies and Provisions for Re-Use, Re-Distribution

There are no economic, political or other embargoes that will be placed on the use of the data, nor privacy or ethical issues that will constrain the release of this data to the general public. Once published and made available in a publicly accessible data storage, the data can be used for any purpose deem fit by any user.

VITA

Emmanuel Atem Njinju

Candidate for the Degree of

Master of Science

Thesis: CRUSTAL AND SUB-CONTINENTAL LITHOSPHERIC MANTLE DECOUPLING BENEATH THE MALAWI RIFT

Major Field: Geology

Biographical:

Education:

Completed the requirements for the Master of Science in Geology at Oklahoma State University, Stillwater, Oklahoma in May, 2016.

Completed the requirements for the Bachelor of Science in Geology at University of Buea, Cameroon in 2012.

Completed the requirements for the Bachelor of Science in Mathematics at Advanced Teachers Training College, Annex Bambili, University of Yaounde 1, Cameroon in 2007.

Experience:

Boone Pickens School of Geology Graduate Teaching and Research Assistant (2014 – 2016).

National Refining Company Limited (SO.NA.RA), Limbe, Cameroon, Production Operator (2013– 2014).

Ministry of secondary education, Government High School Idenau, Cameroon, Mathematics teacher (2008– 2013).

Professional Memberships:

Society of Exploration Geophysicists (SEG)

American Geophysical Union (AGU)

Geological Society of America (GSA)